Biogeochemistry (2025) 168:38
https://doi.org/10.1007/s10533-025-01229-4

Greenhouse gas fluxes from two drained pond sediments: a mesocosm study

Thi Tra My Lang · Lars Schindler · Chihiro Nakajima · Lisa Hülsmann · Klaus-Holger Knorr · Werner Borken

Received: 1 July 2024 / Accepted: 17 March 2025

Abstract Ponds can store large amounts of organic matter (OM) in their sediments, often accumulated over long periods of time. Sediment OM is largely protected from aerobic mineralization under water saturated conditions but are vulnerable when exposed to oxygen during periods of drought. As climate change progresses, drought periods are likely to occur more frequently and may affect OM mineralization, and thus the release of greenhouse gases (GHGs) such as carbon dioxide (CO_2), methane (CH_4) and nitrous oxide (N_2O) from pond ecosystems. Therefore, we aimed to test how GHG emissions and concentrations in the sediment respond to drought by gradually decreasing water levels to below the sediment surface. To this end, undisturbed sediment cores from two small ponds with distinct watershed and water chemistry characteristics were incubated in mesocosms for 118 days at 20 °C. Water levels were sequentially tested at 3 cm above the sediment surface (Phase I) and at the level of the sediment surface (Phase II). In Phase III, water levels were continuously lowered either by evaporation or by active drainage including evaporation. Mean CH_4 fluxes of both ponds were high (21 and 87 mmol m^{-2} d^{-1}), contributing 90 and 96% to the GHG budget over the three phases. The highest CH_4 fluxes occurred in Phase II, while active drainage strongly reduced CH_4 fluxes in Phase III. A multivariate analysis suggests that dissolved organic carbon and sulphate were important drivers of CH_4 fluxes in Phase III. CO_2 and N_2O fluxes also responded to declining water levels,

Responsible Editor: Melanie A. Mayes

Supplementary Information The online version contains supplementary material available at https://doi.org/10.1007/s10533-025-01229-4.

T. T. M. Lang · L. Schindler · C. Nakajima · W. Borken (✉)
Soil Ecology, University of Bayreuth, Dr.-Hans-Frisch-Str. 1-3, 95448 Bayreuth, Germany
e-mail: werner.borken@uni-bayreuth.de

T. T. M. Lang
Thünen-Institute of Climate-Smart Agriculture, Bundesallee 65, 38116 Brunswick, Germany

L. Hülsmann
Ecosystem Analysis and Simulation (EASI) Lab, University of Bayreuth, Dr-Hans-Frisch-Str. 1-3, 95448 Bayreuth, Germany

L. Hülsmann · W. Borken
Bayreuth Center of Ecology and Environmental Research (Bayceer), University of Bayreuth, Dr-Hans-Frisch-Str. 1-3, 95448 Bayreuth, Germany

K.-H. Knorr
Biogeochemistry and Ecohydrology Group, Institute of Landscape Ecology, University of Münster, Heisenbergstr. 2, 48149 Münster, Germany

Published online: 01 April 2025

but their contribution to the GHG budget was rather small. Both gases were primarily produced in the upper sediment layer as indicated by highest concentrations at 5 cm sediment depth. Compaction of sediment cores by water level lowering increased bulk density and maintained high water contents. This side effect, retarding the drying of the sediment surface, was possibly relevant for the GHG net emission of the sediments in Phase II and III. Overall, GHG fluxes from the sediments exhibited high sensitivity to falling water levels. This study suggests that drying pond sediments have great potential to emit large amounts of GHGs to the atmosphere in the event of drought, representing hot spots of GHGs in the landscape.

Keywords Pond sediment · Drainage · Drought · Carbon dioxide · Methane · Nitrous oxide

Introduction

Carbon dioxide (CO_2), methane (CH_4) and nitrous oxide (N_2O) are potent greenhouse gases (GHG) and their atmospheric concentrations have risen sharply since pre-industrial times (IPCC 2021). Projections of future GHG emissions still show large uncertainties with respect to some ecosystems (IPCC 2021), in particular to aquatic ecosystems (Rosentreter et al. 2021). This also applies to shallow inland waters < 5 m (Richardson et al. 2022) which play an important role in the global carbon (C) cycle due to their high abundance (Downing et al. 2006; Tranvik et al. 2009) and which emit substantial amounts of GHGs to the atmosphere (Kosten et al. 2010; Yang et al. 2015; Ma et al. 2018; Yuan et al. 2019). Global climate change may further entail additional uncertainties for the GHG budget of inland aquatic ecosystems. For example, more frequent drought periods increase the area of sediments exposed to aeration in shallow lakes and ponds for extended periods of time (Martinsen et al. 2019; Schmiedeskamp et al. 2021). GHG fluxes of lakes and ponds may respond differently to sediment exposure to aeration, as sediment properties control the production and consumption of GHGs (Tranvik et al. 2009). Yet, little is known about how CO_2, CH_4 and N_2O fluxes respond to the transition from saturated to unsaturated conditions in pond sediments with distinct biogeochemical characteristics.

The biogeochemistry of inland aquatic ecosystems in urban areas is often affected by large inputs of sediments, nutrients and allochthonous organic matter from surrounding terrestrial land (Boyd and Massaut 1999) or by aquaculture (Boyd et al. 2010; Kokou and Fountoulaki 2018). The accumulation of organic matter in sediments additionally relies on detritus inputs from autochthonous production. An average burial rate of organic matter in small eutrophic lakes and ponds was estimated to be around 1000 g C m^{-2} per year, far exceeding the burial rates in larger natural lakes (Downing et al. 2008). A large proportion of organic matter is buried under anoxic conditions in the sediment over the long term (Keiluweit et al. 2017), but substantial organic matter losses may occur upon aeration of sediments in drought periods (Sobek et al. 2009), especially in small aquatic ecosystems with thick and organic-rich sediments. When oxygen (O_2) penetrates the sediment surface it stimulates microbial activity and affects the production and release of GHGs (Jin et al. 2016; Marcé et al. 2019).

There is growing evidence that global CO_2 fluxes from oxygen-exposed inland aquatic ecosystems are underestimated (Raymond et al. 2013; Keller et al. 2020). Compared to inundated ponds, CO_2 fluxes from dry pond sediments were found to be on average 10 times higher under similar climatic conditions (DelVecchia et al. 2021). Oxygen input into sediments in drying periods can turn lakes and ponds from CO_2 sinks into CO_2 sources (Gilbert et al. 2017). This switch is caused by absence of CO_2 fixation by aquatic plants and the penetration of O_2 into the sediment, which drives the aerobic degradation of organic matter (Gilbert et al. 2017). The deeper O_2 penetrates the sediment, the greater the potential for organic matter losses and increasing CO_2 fluxes. The phase of increasing CO_2 fluxes can last for some weeks when the sediment dries out until the onset of rain reduces the O_2 supply (Gilbert et al. 2017). Simulation of increasing desiccation of sediments by extreme droughts suggests a doubling of CO_2 fluxes from Mediterranean fluvial networks (Gómez-Gener et al. 2015). As small and shallow ponds dry out particularly quickly, they have a great potential for CO_2 losses. The water content in the aerated sediment also has a strong influence on the CO_2 flux. At elevated temperatures, high water contents cause evaporative cooling, which reduces CO_2 fluxes from sediments (Martinsen et al. 2019). If the water content is very

low, microorganisms are exposed to drought stress and either die due to desiccation or survive by going dormant (Schimel 2018). The intensity of sediment drying and vertical gradients of sediment water content are therefore important drivers of CO_2 fluxes during dry phases (Fromin et al. 2010).

Waterlogged lake and pond sediments are favorable habitats for methanogenic microorganisms, whereby nutrient availability, quantity and quality of organic matter are crucial factors for CH_4 production in sediments (Beaulieu et al. 2019; Berberich et al. 2020; Praetzel et al. 2020). A part of the produced CH_4 may be consumed by methanotrophs under oxic or also anoxic conditions in the sediment. Anaerobic oxidation of methane (AOM) was confirmed in limnic and terrestrial ecosystems (Smemo and Yavitt 2011; Gauthier et al. 2015; Shen et al. 2020; Fan et al. 2021) and linked with a range of alternative electron acceptors such as nitrate (Haroon et al. 2013), humic acids (Bai et al. 2019), sulfate (SO_4^{2-}) (Valentine 2002), iron and manganese oxides (Beal et al. 2009). The potential of AOM may vary with the occurrence of alternative electron acceptors among sediments. Although different AOM pathways have been identified, it is still unclear whether this process contributes substantially to the consumption of CH_4 in sediments at low water level.

Methane is transported though the water column to the atmosphere mostly via diffusion or ebullition. Ebullition indicates high CH_4 production in the sediment, contributing up to 75 to 96% of the total CH_4 flux from some lakes and ponds (Casper et al. 2000; Almeida et al. 2016; van Bergen et al. 2019; Schmiedeskamp et al. 2021). A significant fraction of CH_4 is consumed by aerobic methanotrophs when travelling through the water column (Bastviken et al. 2008), thereby effectively lowering the CH_4 emission to the atmosphere. As the water level drops and the sediment surface become exposed to aeration, this CH_4 sink disappears, yet methanotrophy may occur in the uppermost sediment layers. Overall, CH_4 fluxes from oxygen-exposed sediments are difficult to predict, as several microbial processes are involved in both CH_4 production and CH_4 consumption (Schmiedeskamp et al. 2021).

The few existing studies on N_2O fluxes from dry sediments show large differences among inland aquatic ecosystems. Both high and low N_2O fluxes from oxygen-exposed sediments were even found on a small scale along a gradient from dried sediments at the shore of a hydroelectric reservoir (Jin et al. 2016). The high spatial and temporal variability of N_2O fluxes is explained by the involvement of different microbial processes that contribute to the production and consumption of N_2O and precursors (Pinto et al. 2021). In N_2O formation by denitrification, nitrate is used as terminal electron acceptor, which enters the system through external water inputs or is formed by nitrification in the sediment if sufficient oxygen is available. Nitrification itself can dominate N_2O formation in the sediment after prolonged drought, which is related to the increasing oxygen supply (Pinto et al. 2021). Thus, ecosystems with high organic matter contents and low C:N ratios are favorable environments for N_2O formation (Wang et al. 2021). High phosphate contents in sediments also may further stimulate N_2O fluxes (Ertürk Arı et al. 2021) as phosphate is often a limiting factor for microbial growth. As many microbial process rates are dependent on the availability of oxygen, the preconditions for N_2O formation can quickly change with small fluctuations in water level in sediments. A better assessment of N_2O fluxes from oxygen-exposed sediments could be significant for the GHG balance of inland aquatic ecosystems because of the high global warming potential of N_2O (IPCC 2021).

Little is known about how declining water table levels affect GHG fluxes from oxygen-exposed pond sediments and how the magnitude of GHG fluxes is related to sediment properties. Additionally, it is unclear if AOM contributes substantially to CH_4 cycling in pond sediments. We hypothesize that declining water table (i) increases CO_2 fluxes, decreases CH_4 fluxes, and increases N_2O fluxes from dry sediments, evoked by rising O_2 availability and microbial respiration in the top sediment layers. We also hypothesize that (ii) in two ponds with distinct watershed and sediment chemistry conditions, there will be pond-specific responses of GHG fluxes to water table decline, related to chemical properties and the abundance of microbial biomass of the sediments. Further, we expect that (iii) AOM rates may differ between ponds and sediment depths due to differences in nitrate and sulfate concentrations as potential electron acceptors.

To test these hypotheses, a mesocosm experiment was conducted over 16 weeks using undisturbed sediment cores from two ponds with water

and sediment input from distinct geological regions and land use intensities. The experiment was divided in three phases: I. water level ~ 3 cm above sediment surface, II. water level at sediment surface, III. water level below sediment surface with two treatments (IIIa) evaporation (control) and (IIIb) active drainage in addition to evaporation. Microbial biomass, chemical and physical parameters of sediment cores were determined after Phase III. AOM rates in sediments were assessed in a complementary incubation approach using $^{13}CH_4$ to assess the production of CO_2 by AOM.

Materials and methods

Site description and sampling

Twenty-six sediment cores were taken from two drained ponds close to the city of Bayreuth, southern Germany, in November and December 2021, about 2–3 weeks after drainage. Ten sediment cores were used for the water level manipulation incubation and three sediment cores per pond for AOM rates (see below). Pond A had an area of 2600 m^2 and was located in Görschnitz (49°57′36''N, 11°42′00''E) at 488 a.s.l. while pond B, located near Creußen (49°52′12''N, 11°36′36''E) at 468 a.s.l., was larger with an area of 9025 m^2. Mean annual temperature was 9 °C and mean annual precipitation was 950 mm in both locations. Continuous water inflow from small streams was dammed up to a height of 2–3 m with a wall in both ponds and led to sedimentation of organic and mineral particles. The thickness of sediments varied between 20 and 80 cm in both ponds. The sediment deposits originated from various soil types in the catchment area that developed from the geological formations of Triassic Shell-Limestone (pond A) and Triassic Keuper-Sandstone (pond B). Land use in the surrounding area was a mixture of grassland, arable land, and forest, with pond B being more surrounded by arable land than pond A.

Plexiglas cylinders (height 30 cm, inner diameter 17.2 cm) were inserted by hand into the sediments to a depth of 25 cm. All Plexiglas cylinders (hereafter sediment core) were sealed on both ends by foam material and lids for transportation. Thereafter, pond water was added to each sediment core 3 cm above the sediment surface to ensure water-saturated conditions. All sediment cores were stored in a climate chamber at 2 °C for five weeks before installation in mesocosms to avoid artefacts from sampling.

Experimental setup

For the incubation experiment, ten sediment cores per pond were installed in a mesocosm system. A mesocosm consisted of a sediment core, a bottom with an integrated water-permeable plate (1 µm pore diameter) and drainage connection, and a lid with two tube connection fittings for ventilation or GHG flux measurements (Fig. S1). Two perforated plastic tubes (17.5 cm length, 1 cm inner diameter) coated by silicone tube (thickness of 1 mm) and equipped with a gas-tight septum served as diffusive equilibration samplers for dissolved gases (Knorr et al. 2008) and were horizontally installed in each sediment core at 5 and 20 cm sediment depth to allow gas sampling using a syringe. Mesocosms were incubated at 4 °C in the dark for one week to eliminate residual O_2 and to mimic in-situ pond conditions at water saturation. Thereafter, mesocosms were incubated at 20 °C and ventilated above the water or sediment surface using atmospheric air with a continuous flow of ~ 450 ml min^{-1} per mesocosm. The experiment took place over 118 days, separated into three phases:

Phase I (days 1–36): water saturation, water level 3 cm above the sediment (n = 10 per pond).

Phase II (days 37–70): water saturation, water level at sediment surface (n = 10 per pond).

Phase III (days 71–118): water level below sediment surface, progressive water loss by evaporation in the control treatment (n = 5 per pond) and active drainage of mesocosms in the drainage treatment (n = 5 per pond).

In Phase I, all mesocosms were kept under water-saturated conditions with a 3 cm water layer above the sediment surface. In Phase II, the supernatant water layer was carefully removed using a syringe. In Phase III, one half of mesocosms was continuously drained by a suction pump, connected to the bottom of the mesocosms. The suction pump was adjusted to a pressure of -300 hPa. Drainage water of mesocosms was collected in glass flasks and weighed at the end of the experiment. Five undrained mesocosms of each pond sediment served as control. Water losses by evaporation or drainage were determined at the

beginning and end of Phase II and III by weighing of mesocosms.

Greenhouse gas measurements

Fluxes and concentrations of CO_2, CH_4 and N_2O were measured separately within three days on a weekly to fortnightly basis during the three phases. Gas fluxes were measured using different portable gas analyzers (CO_2: LI-820, LI-COR Biosciences GmbH, Bad Homburg, Germany; N_2O: LI-7820, LI-COR Biosciences GmbH, Bad Homburg, Germany; CH_4: LGR-ICOS Micro Portable Gas Analyzer, ABB Inc., Quebec, Canada). The ventilation of a single mesocosm was interrupted for the duration of gas measurements. Instead, the headspace of an individual mesocosm was connected to the inlet and outlet tubes of one gas analyzer. All gas analyzers were equipped with a gas pump that circulated the headspace air in the closed system. Flow rates and duration of measurements varied among the gases (3–5 min for CO_2, 10 min for N_2O, 10–30 min for CH_4). Linear increases in headspace concentration were observed for CO_2 and N_2O fluxes. In the case of CH_4, diffusive and ebullitive fluxes were often occurred simultaneously during a measurement. The increase in CH_4 concentration in the headspace was then non-linear, characterized in part by multiple abrupt increases in CH_4 concentration. The measurement time was 30 min when ebullitive fluxes occurred and the difference between the initial and final CH_4 concentration was used to calculate the CH_4 flux. Diffusive CH_4 fluxes showed a strong linear increase in CH_4 concentration over time ($R^2 > 0.95$) with rates < 0.1 mmol CH_4 m^{-2} h^{-1}. To estimate the contribution of ebullition to the total CH_4 flux, the diffusive flux was therefore set at 0.1 mmol CH_4 m^{-2} h^{-1}. GHG fluxes were calculated based on the slope of the linear increase (CO_2, N_2O, CH_4) or total increase (CH_4 ebullition) in gas concentration in the headspace during measurement. GHG fluxes were calculated as follows:

$$F = \frac{\Delta c}{\Delta t} \times \frac{V}{A} \times \frac{1}{M_v} \times k \times \frac{273.15}{T} \times \frac{P}{101.325} \quad (1)$$

where F is the flux rate of CO_2 and CH_4 (mmol m^{-2} h^{-1}) or N_2O (µmol m^{-2} h^{-1}), $\Delta c/\Delta t$ is the rate of change in gas concentration (m^3 m^{-3} h^{-1}) within the headspace, V is the volume (m^3) of the headspace within the mesocosm, A is the surface area (m^2) of the sediment, M_v is the molar volume of CO_2 (0.02226 m^3 mol^{-1}), CH_4 (0.02236 m^3 mol^{-1}) or N_2O (0.02225 m^3 mol^{-1}) at 273.15 K and 101.325 kPa, k is a factor to convert the gas flux from mol m^{-2} h^{-1} to mmol m^{-2} h^{-1} (CO_2 and CH_4) or µmol m^{-2} h^{-1} (N_2O), T is the incubation temperature (K), P is the atmospheric pressure (kPa). Each gas flux was checked for quality assurance to identify incorrect measurements due to technical problems.

Gas samples were collected from the diffusive equilibration samplers at 5 and 20 cm depth using a syringe with a three-way stopcock. After rinsing the syringe with N_2, about 1 ml of gas sample was retrieved and injected into a N_2 flushed 12 ml glass vial (LabCo Limited, Lampeter, Ceredigion, UK) for analysis of CO_2 and CH_4 concentrations. The dilution factor of CO_2 and CH_4 concentrations was calculated based on the difference in gas pressure in the glass vial before and after sample injection.

$$Dilution\,factor = \frac{(Final\,pressure) - (Initial\,pressure)}{(Final\,pressure)} \quad (2)$$

The CO_2 and CH_4 concentrations were analyzed using a gas chromatograph (SRI Model 8610C-GC, USA) equipped with a methanizer, flame ionization detector FID, and a packed column (Molecular Sieve 13X) within 2–3 days after sampling. An aliquot of 100 µl sample was injected into the column. Calibrations were done with the certified standards of 1000 and 10,000 ppm CO_2 and 30 and 1000 ppm CH_4 (Rießner-Gase GmbH, Lichtenfels, Germany).

N_2O concentrations were immediately measured after sampling by direct injection of 0.25 ml gas sample into a 5.1 ml sample loop, equipped with an injection port and a 4-way valve, connected to the N_2O analyzer (LI-7820 LI-COR Biosciences GmbH, Bad Homburg, Germany). The gas circulated in the closed circle for about 1–2 min until a stable N_2O concentration was recorded. A certified 10 ppm N_2O standard (Rießner-Gase GmbH, Lichtenfels, Germany) was used to calibrate the N_2O analyzer. For this purpose, 0.25, 0.50 and 0.75 ml of the N_2O standard were repeatedly measured at each sampling day. The system was flushed with ambient air for about 5 min after each measurement.

Henry's law was used to calculate CO_2, CH_4, and N_2O concentrations in pore water of the sediments. The temperature-dependent Henry's constant at 20 °C was calculated based on equations described in Sander (2015).

$$c_{water} = k_H \times p \quad (3)$$

where c_{water} is the concentration of GHGs in pore water (mmol L^{-1}), k_H is the temperature-dependent Henry constant at 20 °C (CO_2 38.36 mmol L^{-1} atm^{-1}; CH_4 1.55 mmol L^{-1} atm^{-1}; N_2O 28.22 mmol L^{-1} atm^{-1}), p is the gas partial pressure (atm).

To estimate the dissolved inorganic carbon concentration (DIC, mmol L^{-1}), i.e. the sum of c_{water} (Eq. 3) and pH dependent species of H_2CO_3 (HCO_3^-, CO_3^{2-}) was calculated using the Henderson-Hasselbach equation and the equilibrium constants described in Stumm and Morgan (1995) and Praetzel et al. (2020):

$$DIC = c_{water} + c_{water} \times 10^{(pH-6.4)} + \left(c_{water} \times 10^{(pH-6.4)}\right) \times 10^{(pH-10.25)} \quad (4)$$

where, c_{water} is the calculated dissolved CO_2 concentration, the second term represents the HCO_3^- concentration, and the third term represents the CO_3^{2-} concentration, and pH is the pH of pore water.

Physical sediment properties

Before and after the incubation, weight and height of sediment cores were determined to assess the total amount of pore water and the relative compaction of sediments by shrinkage. After Phase III, stainless steel cylinders (100 cm^3 volume, 5 cm height) were successively taken from two depths (5 cm and 20 cm) of sediment cores. The stainless-steel cylinders were saturated with water in a vessel for 72 h to determine total porosity. Then, the water-saturated sediments were weighed and dried at 105 °C until mass constancy. Sediment porosity (cm^3 cm^{-3}) was calculated as the ratio between water loss (cm^3) by drying over the cylinder volume. Bulk density (BD) of sediments (g cm^{-3}) was calculated as the ratio between dry mass (105 °C) over the cylinder volume. Water-filled pore space (WFPS, %) after Phase III was calculated as ratio of total water volume over total pore volume in each sediment core.

Chemical parameters

Chemical parameters of the sediments were analyzed after Phase III. A sediment-to-water ratio of 1:5 (v/v) was applied to measure the pH of sediment samples. The soil slurries were shaken for 45 min at room temperature. The sediment supernatant was measured to determine the sediment pH using a pH meter (WTW, Wellheim, Germany). Dry sediments (60 °C) were ground using a ball mill (Retsch MM 400, Haan, Germany) and then analyzed for total C and N concentrations using a CN analyzer (Vario Max, Elementar Analysensystem GmbH, Hanau, Germany). To determine the organic and inorganic C fractions, dry sediment samples (10 g) were treated with 8 ml deionized water and 3 ml (HCl 10% v/v) to remove carbonates. After drying (60 °C), the remaining organic C fraction was analyzed by the CN analyzer (see above). The inorganic C concentration was calculated from the difference between total and organic C concentration.

The top and bottom sediments of each pond were extracted with 40 ml of deionized water. The supernatant was filtered (cellulose acetate filter, 0.45 µm) to determine the concentrations of dissolved organic carbon (DOC), ammonium (NH_4^+), nitrate (NO_3^-), and sulfate (SO_4^{2-}) from the sediments. A total organic carbon analyzer (multi N/C 2100, Analytik Jena, Germany) was used for the DOC measurement, while ion chromatography (Metrohm 881 Compact IC pro, Herisau, Switzerland) was used for the nitrate and sulfate measurements. Ammonium (NH_4^+) was extracted with 50 ml of KCl (1 M) and measured by flow injection analysis (MLE Dresden, FIA-LAB, Germany).

Microbial biomass

Chloroform fumigation extraction was conducted according to Wu et al. (1990) to determine microbial biomass C (MBC). For this purpose, fresh sediment samples from 5 and 20 cm depth were prepared by removing roots, wood and litter and then passed through a 2 mm sieve. Aliquots of sieved samples were fumigated at room temperature in a desiccator under a chloroform atmosphere for 24 h. Fumigated and non-fumigated subsamples were both shaken overhead with 0.5 M K_2SO_4 for 45 min at 100 rev.

min^{-1} in a solution ratio of 1:10 then were extracted using cellulose acetate filter 0.45 µm. Organic carbon concentrations in the extracts were measured with a CN analyzer (multi N/C 2100, Analytik Jena, Germany). For calculation of MBC, differences between fumigated and non-fumigated C concentrations were corrected by a factor of 0.45 to account for non-extractable microbial C (Joergensen 1996).

Anaerobic oxidation of methane (AOM)

The AOM incubation experiment was conducted separately by collecting samples from three sediment cores of each pond. The sediment cores were water-saturated, with the water level 3 cm above the sediment surface, and stored in a climate chamber at 2 °C for four months to achieve similar anaerobic conditions in all cores. For the AOM incubation, sediment samples were taken at 5 and 20 cm depth and then pooled per depth and pond. For the incubation setup, 130 ml glass bottles (GL 45, Rasotherm GmbH, Taiwan) with wide necks were filled with 10 g of moist sediment and 400 µL of filtered pond water (0.45 µm) using an anoxic glove box with N_2 atmosphere (< 1 ppm O_2, IL-4 GB, Innovative Technology, USA). Gas-impermeable red Chlorobutyl septa and red plastic screw caps were used to seal the incubation bottles. All glass bottles were heat-sterilized at 250 °C in an oven for 4 h before incubation. An O_2 (anaerobic) indicator (Thermo Scientific, Oxoid Ltd., Basingstoke, Hampshire, UK) was attached to the neck of each incubation bottle using silicone glue to confirm that anaerobic conditions prevailed in the microcosms over the incubation. The indicators' color was regularly recorded (pink- aerobic, white- anaerobic). The sediment samples were flushed with N_2 for 10 min before pre-incubation in a N_2-flushed desiccator at 20 °C under dark conditions for seven days to remove residual O_2 via microbial respiration.

AOM rates in sediment samples were determined using ^{13}C labelled CH_4 (99 atom%, Sigma-Aldrich 490,229-1L-EU) and respective controls without ^{13}C labelled CH_4. Prior to incubation, gas mixtures with 60% CH_4 (28.48 atom% ^{13}C or 1.029 atom% for controls), and 40% CO_2 (natural abundance, 1.097 atom% ^{13}C for both treatments) were prepared. The CO_2 concentration was set to 40% to simulate conditions similar to those in the sediment cores. A volume of 10 ml of CH_4 was added to the headspace of each glass bottle (n = 5 with $^{13}CH_4$ enrichment and n = 3 without $^{13}CH_4$ enrichment per depth and sediment) to trace the change in the ^{13}C signature and concentration of CO_2 as affected by anaerobic oxidation of ^{13}C labeled CH_4. All glass bottles were placed in N_2-purged desiccators and incubated in the dark at 20 °C for 48 h. At the end of the incubation, O_2 indicators confirmed persistently anaerobic conditions in all glass bottles. Gas samples were collected at 0 and 48 h after injection of the gas mixture using 2 ml syringes with stopcock (Luer-Lock, B. Braun Melsungen AG, Melsungen, Germany). Gas samples (2 ml) were transferred to N_2-flushed 12 ml glass vials (LabCo Limited, Lampeter, Ceredigion, UK) to measure CO_2 and CH_4 concentrations using a gas chromatograph (see above). A separate set of samples was taken for stable isotope analyses of CO_2. The ^{13}C signature of CO_2 was analyzed using laser-based cavity ring down spectroscopy (G2201-I, Picarro, Santa Clara, Ca, USA) at the University of Münster, Germany. The instrument was regularly calibrated using in-house standards, validated by IRMS certified reference materials. Data are presented as $\delta^{13}C$ values in ‰ with reference to the Vienna Pee Dee Belemnite (VPDB) standard ($^{13}C/^{12}C$ ratio of 0.0111803). The following equation was used to convert $\delta^{13}CO_2$ to ^{13}C atom%.

$$^{13}Catom\% = 100 \times \left(\delta^{13}CO_2 + 1000\right) / \left[\left(\delta^{13}CO_2 + 1000 + \left(1000/R_{(standard)}\right)\right)\right] \quad (5)$$

where $\delta^{13}CO_2$ (‰) is the measured isotopic signature of CO_2 and $R_{(standard)}$ is the VPDP standard (0.0111803).

The AOM rate (nmol CO_2 g^{-1} d.w. d^{-1}) was calculated using the equation after Szal and Gruca-Rokosz (2020):

$$AOM = \Delta^{13}Catom\% \times \Delta CO_2 \times \frac{V_g \times P}{RT \times m \times t} \times k \quad (6)$$

where Δ ^{13}C atom% is the change in the ^{13}C signature of CO_2 during the incubation, Δ CO_2 is the increase in CO_2 concentration (m^3 m^{-3}) during the incubation, P is the pressure in the incubation jar (Pa), V_g is the volume of headspace in incubation jar (m^3), R is the universal gas constant (8.314 m^3 Pa mol^{-1} K^{-1}), T is the incubation temperature (K), m is the dry weight (g) of the sediment, t is the incubation time (d), and k is a factor to convert the gas concentration from mol CO_2 g^{-1} d.w. d^{-1} to nmol CO_2 g^{-1} d.w. d^{-1}.

Statistics

All statistical analyses and figures were performed using the statistical software R version 4.2.3 (R Core Team 2023). The package *ggplot2* (Wickham 2016) were used for data visualization. We used linear mixed models to test for differences in fluxes and concentrations of CO_2, CH_4, and N_2O between phases, treatments and ponds, using the package *glmmTMB* (Brooks et al. 2017). We used random intercepts for 'day of the experiment' and 'mesocosm' (the latter only when comparing between phases) to account for non-independence between observations. Heteroscedasticity was accounted for by allowing dispersion to vary between ponds, phases and treatments, where applicable. All response variables (e.g., fluxes and concentrations) were log- or square-root transformed to improve agreement with model assumptions, which were checked based on simulated residuals using the package *DHARMa* (Hartig 2022). We used the package *emmeans* (Lenth 2024) to make multiple comparisons of GHG fluxes and concentrations at both depths between two pond sediments in different phases and treatments and present Tukey-adjusted p values. The package *sjPlot* (Lüdecke 2023) was used to plot model predictions and print model summary tables (see Table S1–S16).

Principal component analysis (PCA) was conducted on the mean values of Phase III observations to explore the multivariate associations between GHG fluxes, biogeochemical parameters and water loss of the two pond sediments at different treatments (control, drainage) in Phase III (Fig. 4) using the R package *'FactoMineR'* (Lê et al. 2008) and '*factoextra'* (Kassambara and Mundt 2020).

A linear mixed model was also applied to test the difference in AOM rates between pond sediments and depths using the *glmmTMB* package (Brooks et al. 2017) with 'MesoID' considered as a random intercept to account for non-independence of observations. The *emmeans* package (Lenth 2024) was used to perform multiple comparisons of AOM rates between two pond sediments at both depths. The model summary table (Table S16) was created using package *sjPlot* (Lüdecke 2023).

Table 1 Mean (±SE) texture, bulk density (BD), porosity and volume loss (compaction) in the control and drainage treatments of pond sediments (A and B) after Phase III. Texture was determined from a mixture of both treatments

Site	Texture			BD (g cm^{-3})		Porosity (cm^3 cm^{-3})		Compaction (%)	
	Sand (%)	Silt (%)	Clay (%)	Control	Drainage	Control	Drainage	Control	Drainage
Pond A	11.9 ± 3.8	79.7 ± 3.3	4.8 ± 0.1	0.58 ± 0.01	0.62 ± 0.01	0.78 ± 0.00	0.77 ± 0.00	10.7 ± 1.1	15.7 ± 2.0
Pond B	19.6 ± 7.4	69.9 ± 7.3	3.7 ± 0.1	0.67 ± 0.02	0.64 ± 0.03	0.75 ± 0.01	0.76 ± 0.01	9.5 ± 1.5	9.8 ± 1.9

Results

Physical and chemical sediment properties

Both sediments contained high amounts of silt (70–80%), medium amounts of sand (12–20%) and low amounts of clay (4–5%) (Table 1). Final BDs of sediments were lower in both the control and drainage treatments of sediment A as compared to sediment B with drainage having no clear effect on BD. The porosity of the sediments was similar for both sediments and both treatments, but the initial porosity was higher. Sediments had compacted during the second and third phase as indicated by volume losses between 9.5 (A) and 15.7% (B). In Phase II, sediments lost 7.3% (sediment A) and 7.2% (sediment B) of total pore water through evaporation as the headspace of mesocosms was continuously ventilated (Table 2). After Phase III, water losses (WL) were 19.5% (sediment A) and 18.2% (sediment B) in the control and 28.8% (sediment A) and 23.7% (sediment B) in the drainage treatment, indicating high water losses by evaporation in both treatments. Towards the end of Phase III, the water level, visible on the transparent Plexiglas column, dropped to the bottom of the sediment cores (drainage treatment) or 3–5 cm below the sediment surface (control). Final water filled pore space (WFPS) ranged between 73 and 80% and tended to be slightly smaller in the drainage treatment.

Nearly neutral pH values were found for sediment A while sediment B was relatively acidic with pH values < 5.0 (Table 3). In both sediments, the pH slightly increased with depth to 7.5 (sediment A) and 4.9 (sediment B). Organic carbon contents were 4.8% (sediment A) and 3.7% (sediment B) in the top 5 cm, and similarly, microbial biomass C was higher at both depths in sediment A (378 and 305 µg C g^{-1} d.w. at 5 and 20 cm, respectively) than in sediment B (203 and 74 µg C g^{-1} d.w. at 5 and 20 cm, respectively). By contrast, total nitrogen (TN) at 5 cm depth was found higher in sediment B than A. Dissolved organic carbon (DOC) was homogenously distributed in sediment A (both depths 108 µg C g^{-1}), but heterogeneously distributed in sediment B with 145 µg C g^{-1} at 5 cm and 66 µg C g^{-1} at 20 cm depth. We observed clear differences in ammonium, nitrate and sulfate concentrations between sediment A and B and between the two depths (Table 3). Ammonium concentrations were highest in pond B and increased with depth in both sediments. Nitrate concentrations were highest

Table 2 Mean (± SE) absolute and relative water loss in pond sediments (A and B) in Phase II (n = 10) and Phase III (n = 5). Water filled pore space (WFPS) of mesocosms was determined after Phase III. In Phase III, one half of the mesocosms was drained by vacuum pump and one half served as control

Site	Water loss (g)			Water loss (%)			WFPS (%)	
	Phase II	Phase III		Phase II	Phase III		Phase III	
		Control	Drainage		Control	Drainage	Control	Drainage
Pond A	289 ± 5	691 ± 27	1045 ± 53	7.3 ± 0.2	19.5 ± 1.3	28.8 ± 1.3	75.7 ± 3.4	73.2 ± 1.8
Pond B	312 ± 7	707 ± 40	949 ± 90	7.2 ± 0.1	18.2 ± 0.9	23.7 ± 2.3	79.9 ± 0.9	77.6 ± 3.2

Table 3 Mean (± SE) pH, organic carbon (SOC), total nitrogen (TN) and microbial biomass carbon (MBC) contents in sediments and concentrations of dissolved organic carbon (DOC), ammonium, nitrate and sulfate in extracts from sediments at two depths in mesocosms of pond A and B after Phase III

Site	Depth (cm)	pH	SOC (%)	TN (%)	MBC (µg C g^{-1} d.w.)	DOC (µg C g^{-1} d.w.)	NH_4^+ (µg N g^{-1} d.w.)	NO_3^- (µg N g^{-1} d.w.)	SO_4^{2-} (µg S g^{-1} d.w.)
Pond A	5	7.38 ± 0.11	4.8 ± 0.1	0.20 ± 0.01	378 ± 13	108 ± 17	26.7 ± 2.1	163.1 ± 28.2	275.3 ± 15.0
	20	7.48 ± 0.04	4.6 ± 0.1	0.19 ± 0.01	305 ± 25	108 ± 19	114.2 ± 24.9	18.4 ± 12.0	121.1 ± 32.1
Pond B	5	4.66 ± 0.10	3.7 ± 0.1	0.29 ± 0.01	203 ± 19	145 ± 5	50.9 ± 6.8	47.8 ± 12.8	724.5 ± 19.0
	20	4.85 ± 0.04	2.6 ± 0.1	0.24 ± 0.01	74 ± 19	66 ± 6	124.4 ± 5.3	0.1 ± 0.0	273.2 ± 21.2

in sediment A and decreased with depth. Sulfate concentrations were also higher at the top than at the bottom of both sediments. Notably, sediment B contained large amounts of sulfate, being about three times (5 cm) and two times (20 cm) than sediment A.

CO_2 fluxes and concentrations at different water levels

Carbon dioxide fluxes of both sediments increased from about 1 to 4 mmol m^{-2} h^{-1} over the three Phases (without drainage treatment in Phase III) (Fig. 1a). In the first two phases, CO_2 fluxes were overall higher ($p < 0.05$, Table S1) in sediment A than B, but the CO_2 fluxes reversed toward the end of the second Phase with a steady increase in sediment B. At the end of Phase III, CO_2 fluxes of the controls were at a similar level. Drainage had a strong initial positive effect on CO_2 fluxes of sediment A, after which CO_2 fluxes decreased with time ($p < 0.001$, Table S2). Overall, drainage increased CO_2 fluxes by 73% compared to only evaporation in sediment A. By contrast, the drainage treatment had no effect on CO_2 fluxes of sediment B.

DIC concentrations at both depths were many times higher ($p < 0.001$, Table S3-S6) in sediment A than in sediment B during the three phases (without drainage treatment in Phase III) (Fig. 1b, c). High pH values (Table 3) led to high DIC concentrations in pore water of sediment A, which according to Eq. 4 consists of about 90% HCO_3^- (not shown). Drainage reduced DIC concentrations immediately in sediment A, where the decrease was stronger at 5 cm than at 20 cm depth (both $p < 0.0001$, Tables S5, S6). The strong initial decrease in DIC concentration by the drainage treatment coincided with the strong increase in CO_2 flux from sediment A. With some delay, this relation was also observed for the control of sediment A as the water level dropped below the sediment surface by evaporation. At pH values of 4.7 to 4.9 (Table 3), DIC was almost entirely in the form of H_2CO_3/CO_2 (Eq. 4) in sediment B. In Phase III, DIC concentrations decreased in both the control and drainage treatments of sediment B (Fig. 1b, c), but the drainage treatment was not significant at both depths (Table S5, S6). The average proportion of physically dissolved CO_2 (c_{water}, Eq. 3) in DIC (Eq. 4) was 9% in sediment A and 98% in sediment B. Nevertheless, the physically dissolved CO_2 fraction in sediment A was 1.1 to 4.2 times higher than in sediment B during the three phases.

CH_4 fluxes and concentrations at different water levels

Methane fluxes varied between < 0.1 and 11.3 mmol m^{-2} h^{-1} in sediment A and between 0.001 and 3.3 mmol m^{-2} h^{-1} in pond B over the entire experimental period (Fig. 2a). Ebullition contributed on average 98% (sediment A) and 95% (sediment B) to CH_4 fluxes during Phase I and II. In phase III, ebullition was only sporadically observed in a few mesocosms of the control treatment. In contrast, only diffusion with flux rates < 0.1 mmol CH_4 m^{-2} h^{-1} was observed in the drainage treatment. Methane fluxes were significantly higher in sediment A than in B during Phase I ($p < 0.0001$, Table S7) and Phase III ($p = 0.0017$, Table S8), whereas the differences were not significant in Phase II. Sediment A emitted 59% and 66% more CH_4 under water-logged conditions during Phase I and II, respectively, than sediment B. With water loss in the top sediments due to evaporation, CH_4 fluxes of controls decreased from mid of Phase II until the end of Phase III. Drainage significantly reduced CH_4 fluxes of sediments (both $p < 0.0001$, Table S8).

Methane concentrations at 5 and 20 cm depths were higher in sediment A than in B during Phase I and II (all $p < 0.014$, Tables S9, S10) (Fig. 2b, c). It is noteworthy that mean CH_4 concentrations were 44% (sediment A) and 45% (sediment B) higher at 5 cm than at 20 cm depth during Phase I and II, which indicates a very slow recovery of the natural vertical CH_4 concentration gradient in our setup. In Phase III, a decrease in CH_4 concentration occurred in both sediments and depths. Drainage reduced CH_4 concentrations at both depths of sediment A (both $p < 0.0001$, Table S11, S12) while the drainage effect was not significant at 5 cm ($p = 0.718$, Table S11) or weak at 20 cm depth ($p = 0.03$, Table S12) in sediment B.

N_2O fluxes and concentrations at different water levels

Nitrous oxide fluxes of sediment A ranged between 1 and 17 µmol m^{-2} h^{-1} and were significantly higher during Phase I and II (both $p < 0.0001$, Table S13) than of sediment B (0.2 and 2.8 µmol m^{-2} h^{-1})

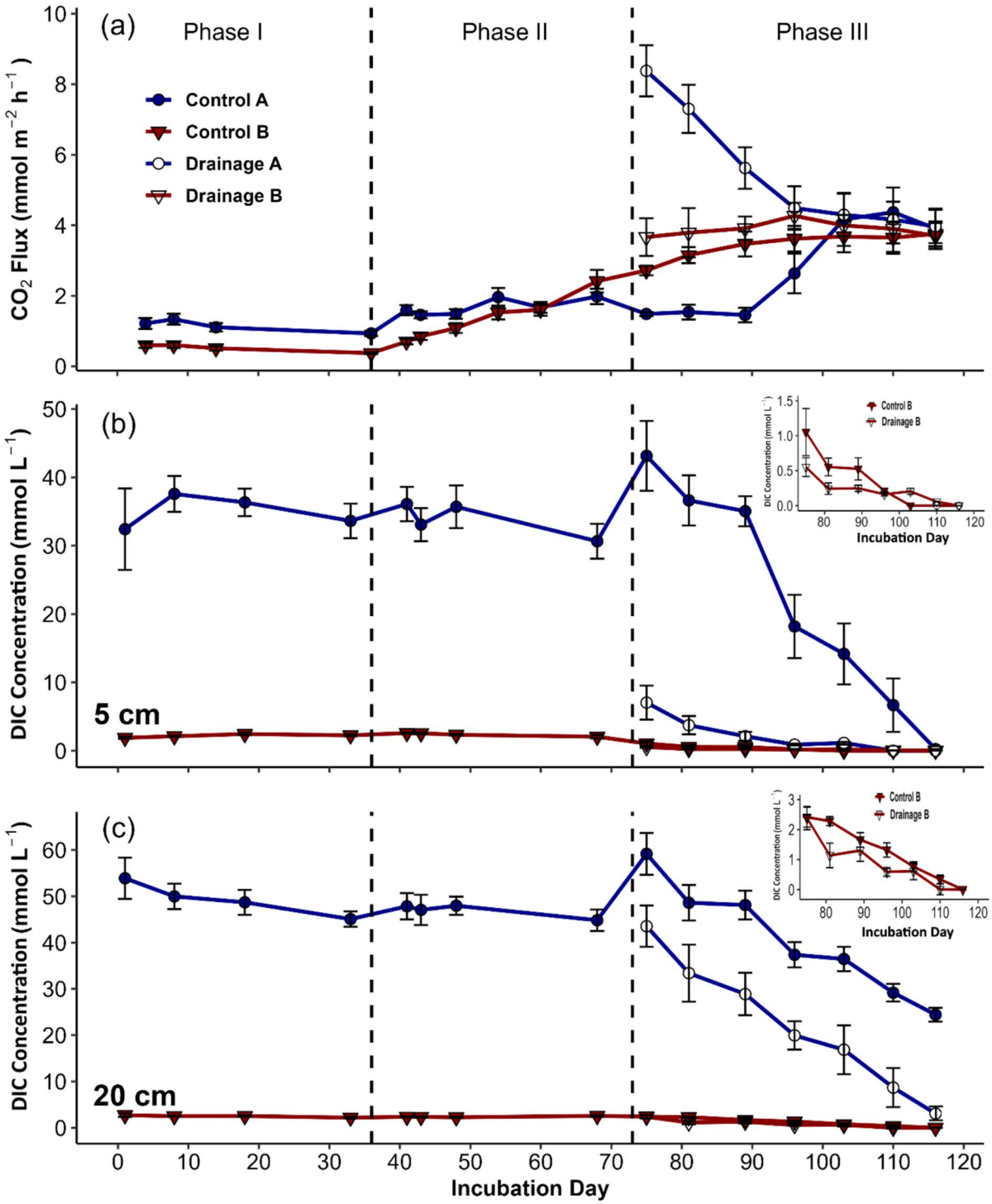

Fig. 1 Mean (±SE) CO_2 flux (**a**) and DIC concentration at 5 and 20 cm depth (**b**, **c**) of two pond sediments (A, B) at different water levels. Phase I: water saturation, water level 3 cm above the sediment surface (n = 10); Phase II: water saturation, water level at sediment surface (n = 10); Phase III: partial water saturation, progressive water loss by evaporation in the control treatments (n = 5) and active drainage of mesocosms in the drainage treatment (n = 5)

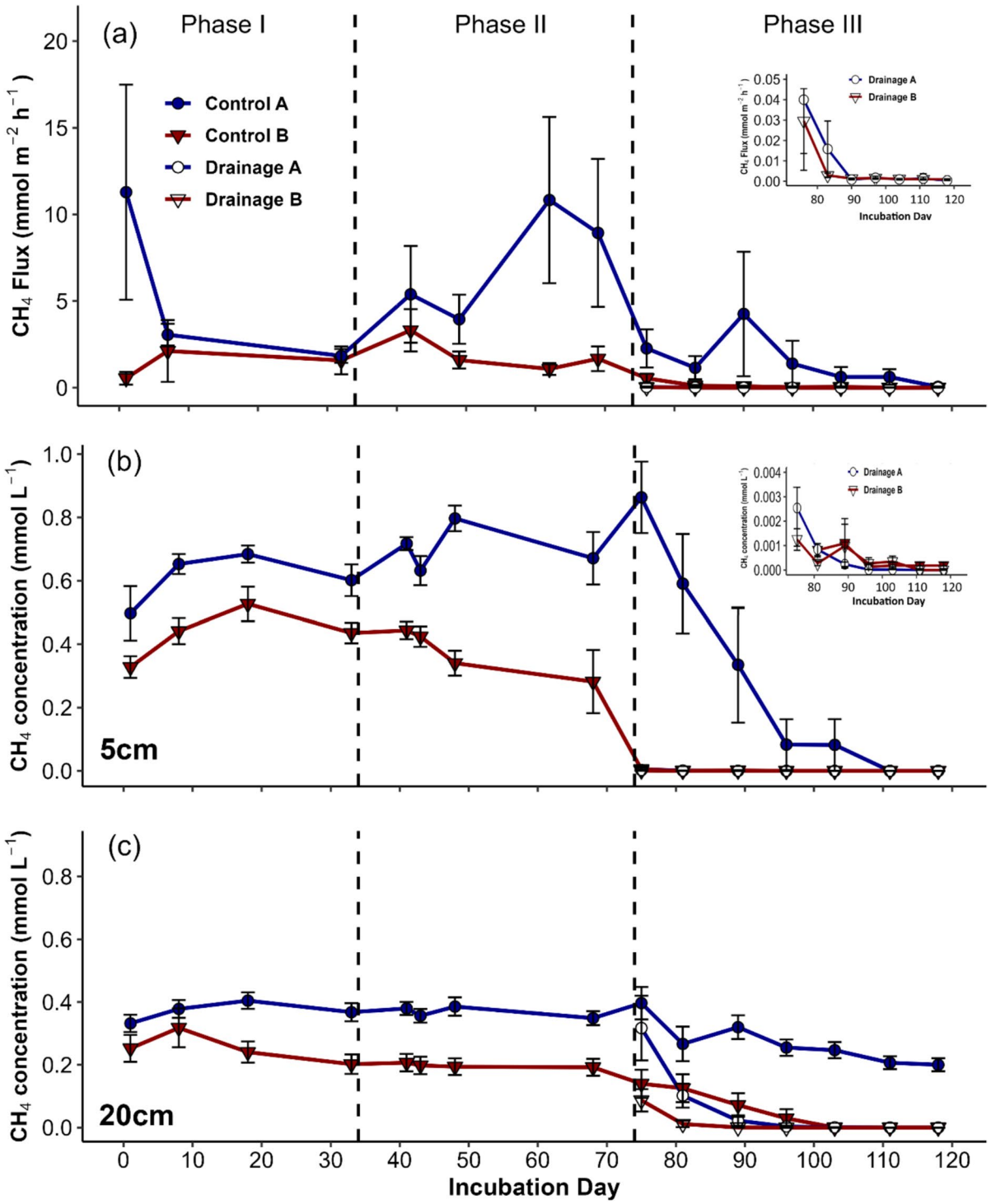

Fig. 2 Mean (±SE) CH_4 flux (**a**) and CH_4 concentration at 5 and 20 cm depth (**b**, **c**) of two pond sediments (A, B) at different water levels. Phase I: water saturation, water level 3 cm above the sediment (n = 10); Phase II: water saturation, water level at sediment surface (n = 10); Phase III: partial water saturation, progressive water loss by evaporation in the control treatments (n = 5) and active drainage of mesocosms in the drainage treatment (n = 5)

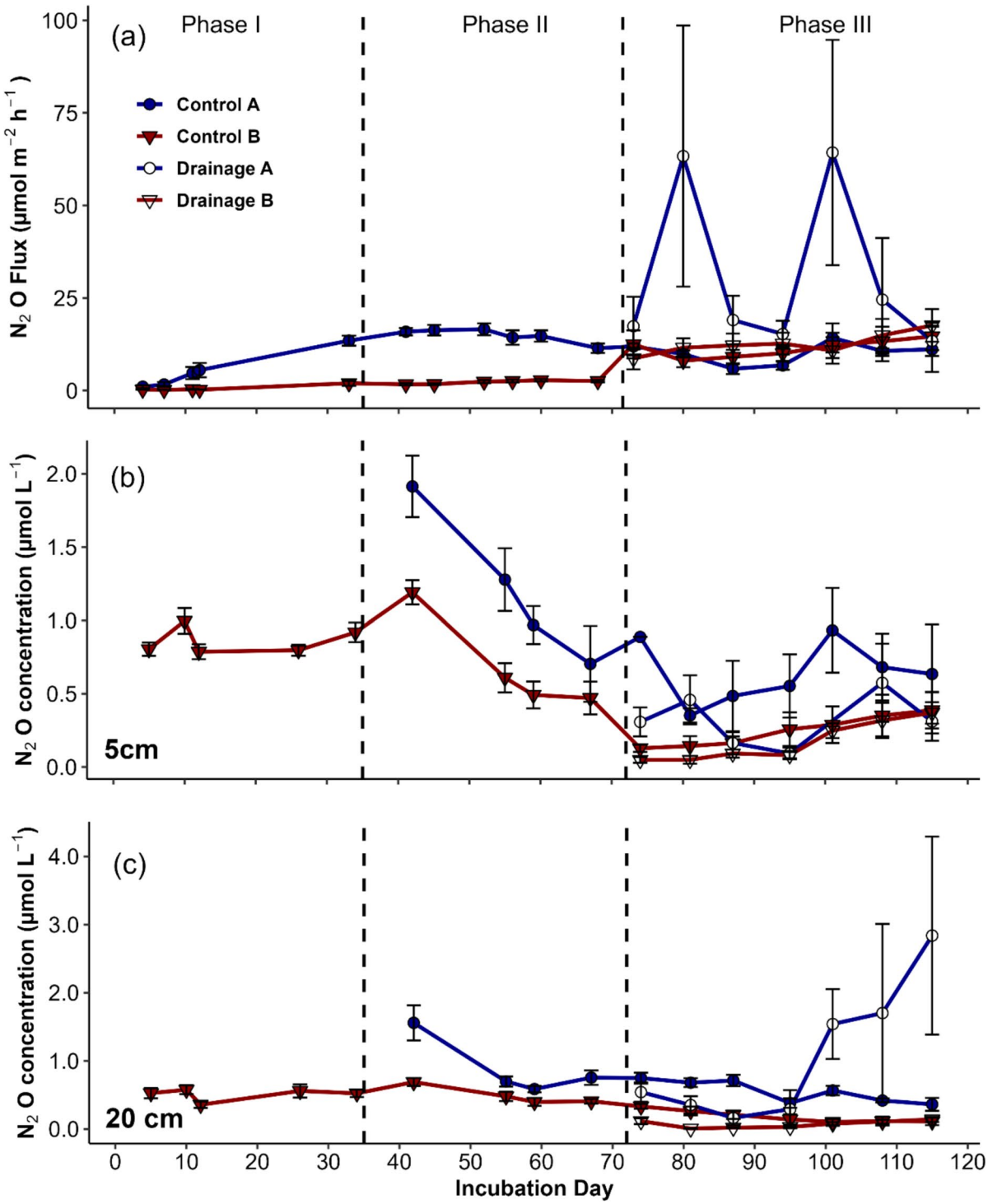

Mean (±SE) N_2O flux (**a**) and N_2O concentration at 5 and 20 cm depth (**b**, **c**) of two pond sediments (A, B) at different water levels. Phase I: water saturation, water level 3 cm above the sediment (n = 10); Phase II: water saturation, water level at sediment surface (n = 10); Phase III: partial water saturation, progressive water loss by evaporation in the control treatments (n = 5) and active drainage of mesocosms in the drainage treatment (n = 5)

(Fig. 3a). The N_2O flux of sediment B increased at the beginning of Phase III and reached a similar level as sediment A, so the sediment controls showed no significant difference in the further course. Maximum N_2O fluxes were observed in sediment A following drainage in Phase III. While drainage had a significant effect on N_2O fluxes of sediment A ($p=0.012$, Table S14), no response was found for sediment B.

Because of the gas composition in pore water (presumably due to excessive H_2S or other interfering components), it was not possible to analyze the N_2O concentrations in sediment A during Phase I (Fig. 3b, c). In Phase II, N_2O concentrations of sediment A were yet higher at both depths than of sediment B. Drainage slightly reduced N_2O concentrations at 5 cm depth in sediment A and B, but the effect was not significant (Table S15). A significant response, however, was observed at 20 cm depth in sediment B ($p=0.0018$, Table S16). In sediment A, lower N_2O concentrations at 20 cm depth were found during the first three weeks after the beginning of the drainage treatment, but thereafter N_2O concentrations increased and reached a maximum of about 3 µmol L^{-1}. Due to trend reversal and high variability among mesocosms, the overall effect of drainage was not significant for N_2O concentrations in the sediments.

Multivariate analysis of GHG fluxes

The PCA of sediment parameters illustrated well-separated clusters for drainage and control treatments of sediment A versus sediment B after Phase III (Fig. 4). Clusters of the control (only evaporation) and drainage treatment were separated for sediment A, while clusters of the drainage and control treatments of sediment B overlapped with little scatter within the clusters. The first two PCA axes explained 74% of the variation in sediment parameters and GHG fluxes. Axis PC1 explained 44% of the variability and was positively driven by several sediment parameters, in particular pH, C:N, MBC, SOC and NO_3^- (5 cm), all with correlation coefficients of $r>0.83$ ($p<0.001$, Table S17). Axis PC1 was also positively correlated with N_2O fluxes ($r=0.64$, $p=0.003$), CO_2 fluxes ($r=0.54$, $p=0.015$), NO_3^- (20 cm) ($r=0.54$, $p=0.013$) and WL ($r=0.52$, $p=0.019$). Moreover, N_2O and CO_2 fluxes were positively associated with WL, NO_3^- (5 cm) and NO_3^- (20 cm) and clustered with the drainage treatment of sediment A (Fig. 4).

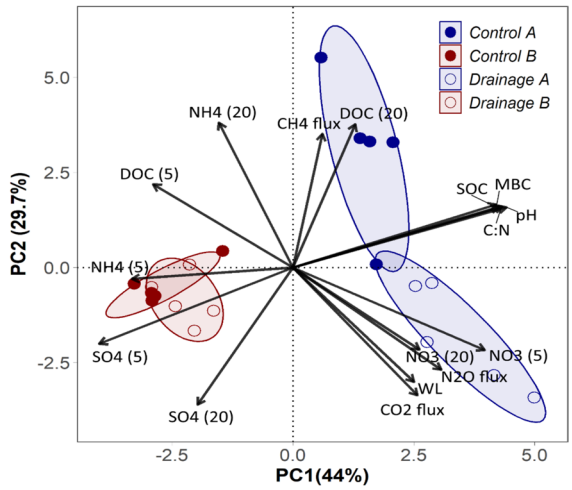

Fig. 4 Principal component analysis (PCA) of greenhouse gas fluxes (CO_2, CH_4, N_2O), water loss and chemical properties of two pond sediments (A, B) including two treatments (Control, Drainage) in Phase III ($n=20$). Each circle represents the mean value of one mesocosm and shapes by different treatments (Control A, Control B, Drainage A, Drainage B). Arrows indicate the variables (DOC, SO_4^{2-}, NH_4^+, NO_3^- at 5 and 20 cm depth, MBC, pH, SOC, C:N and WL of total sediment core) used for the PCA. DOC stands for dissolved organic carbon, MBC for microbial biomass carbon, SOC for soil organic carbon, WL for water loss in Phase III by drainage and/or evaporation

Both GHGs had negative associations with DOC (5 cm) and NH_4^+ (20 cm).

Axis PC2 (Table S17) explained 29.7% of the variation in sediment parameters and GHG fluxes and was positively correlated with NH_4^+ (20 cm), DOC (20 cm), CH_4 fluxes (all $p<0.001$) and DOC (5 cm) ($p=0.044$), and negatively correlated with SO_4^{2-} (20 cm), CO_2 fluxes, WL, N_2O fluxes and NO_3^- concentrations (both depths). CH_4 fluxes were positively associated with DOC concentration (20 cm) and negatively associated with SO_4^{2-} concentration (20 cm). In addition, CH_4 fluxes clustered with the control of sediment A.

Anaerobic oxidation of methane (AOM)

Anaerobic oxidation of methane occurred in sediment A and B at both depths as indicated by positive ^{13}C signatures of CO_2 in the headspace (Table 4). Mean AOM rates were 1.01 and 1.43 nmol CO_2 g^{-1} d.w. d^{-1} at 5 cm depth in sediment A and B, respectively. In both sediments, AOM rates were about 7–8 lower at

Table 4 Mean (±SE) AOM rates, $\delta^{13}C$ of CO_2, increase in $^{13}CO_2$ by AOM at two depths, and total CO_2 production in sediments of pond A and B during separate two-day anoxic incubation

Site	Depth (cm)	AOM rate (nmol CO_2 g^{-1} d.w. d^{-1})	$\delta^{13}C$ of CO_2 (‰)	$^{13}CO_2$ by AOM (at%)	CO_2 production (µmol g^{-1} d^{-1})
Pond A	5 cm	1.01 ± 0.34	38.5 ± 3.8	0.22 ± 0.02	0.50 ± 0.18
	20 cm	0.17 ± 0.03	17.7 ± 2.3	0.14 ± 0.01	0.13 ± 0.03
Pond B	5 cm	1.43 ± 0.34	44.8 ± 6.1	0.24 ± 0.02	0.59 ± 0.13
	20 cm	0.19 ± 0.04	3.3 ± 1.6	0.08 ± 0.01	0.23 ± 0.04

20 cm depth. The AOM rates at the same depth were not significantly different between the two ponds (Table S18). There was a significant difference in AOM rates at 5 and 20 cm in sediment B ($p = 0.008$, Table S18) while no significant depth effect was found for sediment A. Higher AOM rates at 5 cm depth coincided with higher total CO_2 production rates (Table 4) and higher SOC contents (Table 3) as compared to 20 cm depth. Overall, CO_2 production by AOM was relatively small (< 0.3%) compared to total CO_2 production during anoxic incubation of sediments.

Discussion

This study was designed to better understand the fluxes of greenhouse gases from sediments of two ponds with distinct chemical properties at low water levels. The results show that fluxes of CO_2, CH_4 and N_2O from undisturbed sediment cores respond differently to the transition from low waterlogged to unsaturated conditions in the upper sediment. Slight differences in the water level above or below the sediment surface can have a major impact on the GHG balance of inland aquatic ecosystems. Under these boundary conditions, CH_4 fluxes can have a large share in the GHG balance of pond sediments. A nutrient-rich pond sediment with neutral pH exhibited higher CH_4 fluxes as compared to a slightly less nutrient-rich and more acidic pond sediment, suggesting these properties may be important factors associated with CH_4 fluxes.

CO_2 fluxes

Average CO_2 fluxes across the three phases (61.3 and 49.1 mmol m^{-2} d^{-1} in sediment A and B, respectively) were in the lower to medium range compared to other studies. In a review, Marcé et al. (2019) reported CO_2 fluxes of 44–569 mmol m^{-2} d^{-1} from sediments of different dry inland aquatic ecosystems. A large variability (22–703 mmol m^{-2} d^{-1}) was also observed in dry ponds by Martinsen et al. (2019), with partly lower CO_2 fluxes than in our study. The low-medium CO_2 fluxes in our study may be related to the fact that the sediments were not fully drained or aerated at the end of the experiment.

Our first hypothesis that gradual water loss with finally unsaturated conditions in the upper sediment increased CO_2 fluxes was confirmed for both pond sediments. The increase in CO_2 fluxes by a factor of ~ 3 (sediment A) and ~ 7 (sediment B) from Phase I to Phase III shows how sensitive C mineralization responded to water level lowering close to the sediment surface. In line with our experiment, CO_2 fluxes from pond sediments including plants also increased with drying intensity from -53 to 316 mmol m^{-2} d^{-1} within 12 days (Gilbert et al. 2017). The increasing penetration of oxygen into dry sediments is typically regarded as key driver for rising CO_2 production (Jin et al. 2016; Holgerson 2015). We did not measure the O_2 concentration in the sediments, but the visible formation of iron oxy-hydroxides on parts of the aggregate surfaces indicates the penetration of O_2 into the sediments during Phase III (not shown). However, even after the active drainage treatment (Phase III), WFPS was still very high at 73–78%, which indicates a low hydraulic conductivity, low diffusivity, and incomplete O_2 penetration of the entire pore system. At the end of Phase III, control and drainage treatments exhibited similar WFPS and CO_2 fluxes although the water level in the controls was 4–6 cm below the sediment surface. This discrepancy between WFPS and water level could be related to

the drainage, which could have mainly removed free water between the edge of the sediment core and the Plexiglas wall. Maximum respiration rates are typically observed at WFPS of about 60% in soils (Parkin et al. 1997; Fairbairn et al. 2023). Consequently, microbial respiration was likely limited in parts of the sediment cores at WFPS of 73–80% in both control and drainage treatments. Such high WFPS could indicate anaerobic microsites, which have been identified as stabilization mechanism for organic matter even in drained soils due to low C mineralization (Keiluweit et al. 2017). On the other hand, low water contents by extreme drought events can also lead to limitation of microbial activity and a decrease in CO_2 fluxes from sediments (Gómez-Gener et al. 2015).

A short-lived CO_2 boost was found in sediment A at the beginning of the drainage treatment (Phase III). There is evidence that this boost cannot be explained solely by an increase in C mineralization. In contrast, CO_2 flux increased moderately and consistently in sediment B following drainage. We attribute the CO_2 boost in sediment A mainly to the outgassing of dissolved CO_2 from pore water as the CO_2 concentration at 5 cm depth immediately dropped with drainage. With some delay, the DIC concentration including the physically dissolved CO_2 fraction also decreased at a depth of 20 cm. A large pool of dissolved inorganic C (DIC), consisting mainly of bicarbonate and carbonate, can build up in pore water at pH values > 6.2. The comparison between sediment A (pH ~ 7.4) and B (pH ~ 4.7) shows the great influence of pH on DIC storage in pore water of sediments. The rapid outgassing of CO_2 with drainage results from the increasing contact surface area and the CO_2 concentration gradient between pore water and atmosphere. A decrease in pH by oxidation processes releases additional CO_2 by shifting the pH-dependent balance between the DIC species (Eq. 4). CO_2 outgassing also took place in the control of sediment A, albeit weaker and over a longer period due to the lower water loss through evaporation. Like our study, high CO_2 outgassing rates across water–air interface are also reported from riverine ecosystems with input of DIC enriched groundwater from carbonate bedrock (de Montety et al. 2011; Zeng et al. 2011). Taken together, CO_2 outgassing of DIC from drained sediments is a time-limited process that depends on the sediment thickness and the dimension of air-filled pore space which is in exchange with the atmosphere. The current CO_2 production by C mineralization runs in parallel and contributes only a certain part to the overall CO_2 flux from sediments with high pH values, in which large pools of HCO_3^- prevail. In contrast, the CO_2 flux from acidic sediment B is closely linked in time to C mineralization. This differentiation is important to estimate the actual loss of organic C during drainage or drying of sediments.

Observed differences in CO_2 fluxes between sediment A and B across the three phases confirm our second hypothesis that CO_2 fluxes of ponds with distinct watershed and sediment chemistry respond differently to water table decline. Higher CO_2 fluxes coincide with higher OC and MBC contents in sediment A. Average OC contents of 4.7% (sediment A) and 3.2% (sediment B) are in the medium range compared to other lake sediments. Woszczyk et al. (2011) reported a mean OC concentration of 10.7% (range 0.3–18.5%) for eutrophic shallow lakes. In another study, OC contents varied between 0.5 and 5.4% in 24 of 27 lake sediments, though high OC contents of 21–31% have been also reported (Sobek et al. 2009; Schmiedeskamp et al. 2021). In addition to higher SOC contents, greater potential for C mineralisation under aerobic conditions is also indicated by lower N contents or higher C:N ratios in sediment A compared to sediment B. Long-term stabilisation of organic matter in repeatedly dry sediments may be achieved at C:N of 6–10, that typically occurs in well-drained upland subsoils (e.g., Kramer et al. 2017). Increasingly intensive drought periods could thus cause massive CO_2 losses from pond sediments, thereby reducing their sink function for organic C.

CH_4 fluxes

Ebullition was the prevailing transport mechanism and led to high variability of CH_4 fluxes on individual measurement dates during Phase I and II and occasionally also in the controls during phase III. Average CH_4 fluxes of 155 and 42 mmol m^{-2} d^{-1} from sediment A and B, respectively, during Phase I and II indicate high potential of methanogenesis at water saturated conditions in both ponds. A cross-continental survey revealed an average CH_4 flux of < 1 mmol m^{-2} d^{-1} for pond systems (Paranaíba

et al. 2022). However, high CH_4 fluxes similar to our results were also found in another study. The estimated CH_4 flux from the sediment of a waterlogged eutrophic pond was 87 mmol m^{-2} d^{-1} at 25 °C (van Bergen et al. 2019). The shallow or missing water column above the sediment surface (Phase I and II) minimized or excluded the opportunity for CH_4 oxidation in the water column. For example, in lakes, up to 80% of the CH_4 from sediments can be oxidized by methanotrophs in the water column (Bastviken et al. 2008).

In our experiment, CH_4 fluxes decreased with falling water level across the three phases confirming hypothesis 1. An exception was observed for sediment A in Phase II where CH_4 fluxes remained at a high level, indicating persistent methanogenesis despite removal of excess water above the sediment surface. In Phase III, the greater decline of CH_4 fluxes in the drainage treatment emphasizes the sensitivity of CH_4 fluxes to relatively small changes in water level near the sediment surface. It is noteworthy that the controls in Phase III with 1.5 (sediment A) and 0.1 (sediment B) mmol CH_4 m^{-2} h^{-1} still represent net CH_4 sources.

High CH_4 concentrations at 5 cm depth during Phase II indicate maximum CH_4 production in the top layer of both sediments. Relative constant CH_4 production rates can be assumed as CH_4 concentrations showed only weak temporal dynamics at 5 and 20 cm depth during Phase I and II. Drainage and thus deeper penetration of oxygen into the sediment (Yang et al. 2013; Zhao et al. 2020) probably led to a gradual decrease in CH_4 production during Phase III. Outgassing of the existing CH_4 pool, indicated by CH_4 concentrations in the sediment at the beginning of Phase III (Fig. 2b, c), could have contributed to the CH_4 flux during the first days of drainage. However, as the drainage treatment progresses, it becomes clear that CH_4 production has continued to take place at a lower level.

A decline of CH_4 fluxes following drainage was also observed in several other wetland ecosystems (e.g., Hatala et al. 2012; Yang et al. 2013; Pandey et al. 2014; Haque et al. 2015; Zhao et al. 2020; Schmiedeskamp et al. 2021; Tuyishime et al. 2022). Declining CH_4 fluxes are not only driven by decreasing CH_4 production and but also by increasing CH_4 oxidation in drained sediments. Substantial aerobic CH_4 oxidation takes place in air-filled pores as low diffusive transport of oxygen in water limits its availability in water-filled pores (Jacquemin et al. 2006; Elberling et al. 2011). The relative proportion of air-filled pores increased with increasing water loss in Phase III, however, at the same time water loss also compacted the sediment and reduced its total porosity. Such compaction processes of sediments are known from large-scale groundwater lowering in river deltas (Teatini et al. 2011). Due to the compaction, water-filled pore space remained high, i.e., between 73 and 80% in the control and drainage treatments at the end of Phase III. In addition, aggregates were formed in the upper sediment core that were partly covered by an iron oxy-hydroxide coating (not shown), indicating oxic conditions on the aggregate surface. On the other hand, anoxic conditions could still have prevailed inside the aggregates, allowing ongoing CH_4 production. Methane oxidation within the sediments could have contributed to the decline in CH_4 fluxes. A review suggests that between 60 and 90% of produced CH_4 can be consumed by methanotrophs during the diffusive passage through oxic sediment layers (Le Mer and Roger 2001). Methane consumption might be in a similar range in our experiment as some pores were drained down to the sediment bottom.

Methane fluxes differed between sediment A and B likely due to distinct SOC contents and C:N ratios, confirming the second hypothesis. SOC is considered a pivotal driver of methanogenesis, where both the quantity and quality of SOC are critical for the level of CH_4 production (Berberich et al. 2020, Praetzel et al. 2020). Production of aquatic plant litter and external input of plant litter with low availability of inhibitory phenols may increase methanogenesis in lake sediments (Emilson et al. 2018). We did not study phenol availability in the sediments, but quality and quantity of organic matter in our ponds may have been shaped through soil input from eroded arable land. The C:N ratios of 12.8 and 10.8 in sediment B suggest an already strong decomposition history of organic matter, similar to topsoils of arable land with C:N ratios of ~ 11 (Hamer et al. 2008). In the catchment of pond B, a large part of the land is under arable use, while pond A is mainly surrounded by grassland and forest. The deviating C:N ratios in sediment A and B are therefore possibly related to different sources of organic matter. The sediment of pond A, characterized by an almost uniform C:N ratio of 24 and higher SOC content, indicates a higher potential

for microbial utilization including methanogenesis. Weakly decomposed organic matter has typically large portions of cellulose and hemicelluloses, which can be fermented to low-molecular organic acids under anoxic conditions (Huffman 2003; Zheng et al. 2019). Taken together, the SOC content and the C:N ratio of organic matter are critical drivers of methanogenesis in our sediments.

The pH also differed between the two sediments, but we cannot infer a causal relationship with CH_4 fluxes in our study. Yet, there are hardly any systematic studies on the influence of pH on CH_4 fluxes from lake or pond sediments. Methane fluxes from 14 freshwater lake sediments did not correlate with pH (range of 4.1–8.3), although pH affected the community structure of methanogens (Bertolet et al. 2019). Another study showed that pH of lake sediments does not control CH_4 fluxes (Bertolet et al. 2022). Thus, a direct influence of pH on CH_4 fluxes from lake and pond sediments appears to be low.

Pore water chemistry after Phase III provides additional information on controls of methanogenesis. In agreement with other studies (e.g., Bertora et al. 2018; Kim et al. 2020; Hu et al. 2022; Yu et al. 2023), DOC concentration at 20 cm depth and CH_4 flux are positively correlated. Under anoxic conditions, low molecular weight organic acids (LMWOA) from fermentation of plant litter represent a substantial fraction of DOC and are considered an important driver of methanogenesis (Mathijssen et al. 2019). We did not analyze LMWOA and can only speculate that a different DOC composition led to higher CH_4 fluxes in sediment A, as mean DOC concentrations were similar in both sediments. With increasing penetration of O_2 in the upper sediment, DOC may be consumed by other microorganisms (e.g., denitrifiers, sulfate and iron reducers), which have higher energy gain than methanogens (Castro et al. 2000; Muyzer and Stams 2008; Czatzkowska et al. 2020). The negative correlation between sulfate concentration at 20 cm and CH_4 flux agrees with earlier observations that high levels of sulfate suppress CH_4 production (Achtnich et al. 1995; Kumaraswamy et al. 2001). In addition to lower substrate quality of organic matter, the 2–3 times higher sulfate concentrations could explain lower CH_4 fluxes from sediment B compared to sediment A.

Anaerobic oxidation of methane (AOM)

In the third hypothesis, we hypothesized different AOM rates in the sediments of pond A and B and at the two depths due to different concentrations of potential electron acceptors such as nitrate and sulphate. However, this hypothesis was only partly confirmed as AOM rates were not different between the two ponds. Presumably, factors other than the concentration of electron acceptors limited the AOM rates in the sediments. A significant difference in the AOM rates was only recognizable between the two depths of sediment B. Higher AOM rates coincided with higher CH_4, sulfate and nitrate concentrations at 5 cm depth. This is in line with earlier observations that AOM is linked to the availability CH_4 and alternative electron acceptors in the absence of O_2 (Smemo and Yavitt 2007, 2011; Blazewicz et al. 2012; Gauthier et al. 2015). Alternative electron acceptors are formed in the presence of oxygen and, if water-soluble, can spread in pore water by diffusive transport. The formation of alternative electron acceptors at the oxic sediment surface and diffusion into underlying anoxic zones could explain the higher potential for AOM at 5 cm compared to 20 cm depth.

AOM rates of both sediments were low (1.0 and 1.4 nmol g^{-1} d^{-1} at 5 cm depth), but close to AOM rates reported for another lake sediment (1.5 nmol g^{-1} d^{-1}) (Vigderovich et al. 2022) and freshwater sediment (1.05 nmol g^{-1} d^{-1}) (Shen et al. 2020). Considerable higher AOM rates were found in peatlands (23–410 nmol g^{-1} d^{-1}) (Gupta et al. 2013) and paddy soils (7–21 nmol g^{-1} d^{-1}) (Mohanty et al. 2013; Fan et al. 2021). We can only speculate about the reasons for low AOM rates in our pond sediments. The observed high CH_4, sulfate and nitrate concentrations would potentially allow for higher AOM rates. Another potential pathway of AOM is coupled to the reduction of oxidized humic substances (Smemo and Yavitt 2011), which could trigger higher AOM rates in peatlands and other organic-rich wetlands. Ettwig et al. (2016), Mohanty et al. (2017), and Beal et al. (2009) reported that also Fe^{3+} and Mn^{4+} could act as electron acceptors for AOM. The aggregate surfaces, some of which were heavily coated with Fe hydroxides/oxides after phase IIII, indicate a high availability of Fe^{3+} in the sediments. If CH_4 availability and alternative electron acceptors did not limit AOM, low activity of methanotrophs could explain low AOM

rates. The community of methanotrophs is possibly not well adapted to fluctuations in water table in our pond sediments as compared to peatlands and paddy soils. It remains open whether more frequent lowering of the water level with temporary oxic conditions in the upper sediment would lead to higher AOM rates.

Collectively, AOM would reduce total CH_4 fluxes of sediment A and B by 0.3 and 2.1%, respectively. These values are subject to great uncertainty, as the availability of alternative electron acceptors was not controlled in this approach and may deviate from in-situ conditions in the sediments. Fan et al. (2019) found that aerobic methane oxidation was about 250 times higher than average AOM in terrestrial ecosystems. Hence, AOM makes a minor contribution to total CH_4 consumption while aerobic CH_4 oxidation is the prevailing process that reduces CH_4 fluxes in the pond sediments. Thus, lowering the water column above the sediment reduces the potential for AOM.

N_2O fluxes

Mean N_2O fluxes from sediment A (173 µmol m^{-2} d^{-1}) and sediment B (60 µmol m^{-2} d^{-1}) across the three phases were relatively high compared to other oxygen-exposed sediments of inland aquatic ecosystems. Higher N_2O fluxes (240–680 µmol m^{-2} d^{-1}) were found in subtropical and tropical regions or only during short-term events in colder climates as reviewed by Pinto et al. (2021). Temperature is an important driver in N_2O production as shown by sharply rising N_2O fluxes with increasing temperature from 13 to 20 °C in pond sediments (Stadmark and Leonardson 2007). Thus, the incubation temperature of 20 °C in our experiment may have resulted in higher N_2O fluxes than under in-situ conditions.

Another important driver of N_2O fluxes is the decreasing water content in sediments (Ertürk Ari et al. 2021; Pinto et al. 2021), which may alter microbial process rates of the N cycle (Arce et al. 2018; Fromin et al. 2010). Our hypothesis that N_2O fluxes increase with decreasing water level from Phase I to III was largely confirmed. Only N_2O fluxes from sediment A tended to decrease from Phase II to III. However, the drainage treatment in Phase III led to overall higher N_2O fluxes from both sediments, with some very high fluxes from sediment A. We attribute this increase to the amplified mineralization of organic matter stimulated by higher O_2 availability in the upper sediment. Denitrification and nitrifier denitrification are predominant at low O_2 availability whereas nitrification is an aerobic process and relies on high O_2 supply (Wrage et al. 2001). All three processes may have contributed to N_2O production in the sediments as large gradients in O_2 availability can be assumed between air-filled and water-filled pores. Vertically decreasing N_2O concentration indicates that most N_2O was produced in the upper sediment. The high nitrate concentration in the upper sediment may be evidence of N_2O formation through nitrification as well as denitrification. Without competition from plants, denitrifiers can consume a large proportion of the available nitrate, which is transported over short distances to anoxic zones by diffusion in pore water. High nitrate concentration can not only enhance denitrification including N_2O production, but also dissimilatory nitrate reduction to ammonium (DNRA). This anaerobic process competes with denitrification and can utilize nitrate in a similar magnitude as denitrification (Rogers et al. 2021). However, we cannot assess the relevance of DNRA for N turnover in the sediments as we have not measured the process.

Higher N_2O fluxes from sediment A during phases I and II confirm the second hypothesis, according to which the N_2O flux is mainly controlled by the microbial availability of organic matter. Sediment A is characterized by higher SOC contents, microbial biomass, pH and has greater potential for nitrification, as shown by higher nitrate levels after Phase III. However, N_2O fluxes were not different between controls of sediment A and B during Phase III, which may be due to the lower statistical power of five replicates. Only the drainage treatment in Phase III resulted again in higher N_2O fluxes in sediment A than B. The average N_2O flux from the drained sediment A was driven by a few single events (n = 5) with extremely large fluxes (74–196 µmol m^{-2} h^{-1}) on different days and in different mesocosms, contributing 50% to the average N_2O flux (31 µmol m^{-2} h^{-1}). Highly fluctuating N_2O fluxes occur frequently (Ertürk Ari et al. 2021) and result from short-term changes of biogeochemical parameters and microbial processes involved in the N_2O formation. High temporal resolution measurements are needed to capture extreme N_2O fluxes more accurately and to obtain a more

precise estimate of the N_2O budget of drained pond sediments.

GHG budget

Based on the global warming potential for CO_2 (1), CH_4 (27) and N_2O (273) over 100 years (IPCC 2021), CH_4 fluxes dominated the GHG budget with contributions of 96 and 90%, followed by CO_2 fluxes (3 and 8%) and N_2O fluxes (< 3%) in sediment A and B, respectively, throughout the incubation. Such high proportions of CH_4 in the GHG budget are rather atypical for inland water systems, as most studies reported higher CO_2 than CH_4 fluxes (e.g., Casper et al. 2000; Holgerson & Raymond 2016; van Bergen et al. 2019). However, average CH_4 fluxes were 1.4 (sediment A) and 0.7 (sediment B) times the CO_2 fluxes. We cannot exclude that CH_4 fluxes were overestimated during Phase I and II, since ebullition occurred irregularly during the measurements. Despite uncertainties in the detection of ebullitive fluxes, eutrophic pond sediments at low water levels and summer temperatures represent a significant source of CH_4 that can contribute substantially to the GHG budget of a landscape.

Limitations of the study

In this mesocosm experiment, we used undisturbed cores from the top sediment of two ponds and simulated decreasing water levels at constant temperature (20 °C) over four months. The experiment can only mimic a potential scenario for GHG fluxes from the two ponds under field conditions during dry-hot summer months. In-situ GHG fluxes could be even higher at low water levels close to the sediment surface, considering that deeper sediment layers below 25 cm depth can contribute to GHG fluxes. In addition, higher temperatures > 20 °C can further amplify GHG fluxes. It remains open to what extent the incubation length of four months affected the GHG fluxes. Changes in the availability of organic matter or in pore water chemistry could have altered GHG fluxes towards the end of incubation. The time during which the water level is lowered can have a significant impact on GHG fluxes, as the active microbial community must adapt to the new redox conditions. Experimental manipulations of water level under field conditions and monitoring of seasonal GHG fluxes would provide a more robust estimate of the GHG budget of eutrophic ponds in dry-hot summers.

Conclusions

This study suggests that particularly eutrophic sediments of small ponds represent hotspots for CH_4 emissions under slightly waterlogged or partly drained conditions. Maximum CH_4 fluxes may occur when the water-saturated sediment is in direct exchange with the atmosphere. At the same time, relatively small amounts of CO_2 are emitted from sediments, making methanogenesis an important pathway of C losses under these conditions. AOM appears to contribute little to the reduction of CH_4 emissions from pond sediments. Partly drained pond sediments are also potent sources of N_2O, but its proportion to the GHG budget of the sediments is apparently small. Eutrophic ponds can emit large amounts of CH_4 at very low water levels and thus change the greenhouse gas budget at the regional landscape scale.

Acknowledgements We thank Uwe Hell and Karin Söllner for technical assistance in the field and in the laboratory, and the Central Analytical Department of the Bayceer for chemical analyses. We are grateful to Daniel Brügemann and Jonas Kurth for laboratory assistance at the central laboratory at the Institute of Landscape Ecology, headed by Dr. Tanja Broder. We would also like to thank the two anonymous reviewers and the subject editor for their many excellent suggestions, which greatly improved the manuscript.

Author contributions TTML, LS, CN: performed the research and analyzed the data; LH: carried out statistical analyses; KHK: provided instrumental facilities and isotopic analyses; WB and KHK: designed the study. TTML and WB: wrote the paper with contributions from all authors.

Funding Open Access funding enabled and organized by Projekt DEAL. The study was funded from various resources of the University of Bayreuth.

Data availability The data are available in the repository of the University of Bayreuth: https://doi.org/10.57880/rdspace-ubt-4

Declarations

Competing interests The authors have no relevant financial or non-financial interests to disclose.

References

Achtnich C, Bak F, Conrad R (1995) Competition for electron donors among nitrate reducers, ferric iron reducers, sulfate reducers, and methanogens in anoxic paddy soil. Biol Fert Soils 19:65–72. https://doi.org/10.1007/bf00336349

Almeida RM, Nóbrega GN, Junger PC et al (2016) High primary production contrasts with intense carbon emission in a eutrophic Tropical Reservoir. Front Microbiol. https://doi.org/10.3389/fmicb.2016.00717

Arce MI, von Schiller D, Bengtsson MM et al (2018) Drying and rainfall shape the structure and functioning of nitrifying microbial communities in riverbed sediments. Front Microbiol. https://doi.org/10.3389/fmicb.2018.02794

Bai YN, Wang XN, Wu J et al (2019) Humic substances as electron acceptors for anaerobic oxidation of methane driven by ANME-2d. Water Res 164:114935. https://doi.org/10.1016/j.watres.2019.114935

Bastviken D, Cole JJ, Pace ML, Van de Bogert MC (2008) Fates of methane from different lake habitats: connecting whole-lake budgets and CH4 emissions. J Geophys Res-Biogeo. https://doi.org/10.1029/2007jg000608

Beal EJ, House CH, Orphan VJ (2009) Manganese- and iron-dependent marine methane oxidation. Science 325:184–187. https://doi.org/10.1126/science.1169984

Beaulieu JJ, DelSontro T, Downing JA (2019) Eutrophication will increase methane emissions from lakes and impoundments during the 21st Century. Nat Commun. https://doi.org/10.1038/s41467-019-09100-5

Berberich ME, Beaulieu JJ, Hamilton TL et al (2020) Spatial variability of sediment methane production and methanogen communities within a eutrophic reservoir: importance of organic matter source and quantity. Limnol Oceanorg 65:1336–1358. https://doi.org/10.1002/lno.11392

Bertolet BL, West WE, Armitage DW, Jones SE (2019) Organic matter supply and bacterial community composition predict methanogenesis rates in temperate lake sediments. Limnol Oceanorg 4:164–172. https://doi.org/10.1002/lol2.10114

Bertolet BL, Louden SI, Jones SE (2022) Microbial community composition, and not pH, influences lake sediment function. Ecosphere. https://doi.org/10.1002/ecs2.4091

Bertora C, Cucu MA, Lerda C et al (2018) Dissolved organic carbon cycling, methane emissions and related microbial populations in temperate rice paddies with contrasting straw and water management. Agr Ecosyst Environ 265:292–306. https://doi.org/10.1016/j.agee.2018.06.004

Blazewicz SJ, Petersen DG, Waldrop MP, Firestone MK (2012) Anaerobic oxidation of methane in tropical and boreal soils: Ecological significance in terrestrial methane cycling. J Geophys Res-Biogeo. https://doi.org/10.1029/2011jg001864

Boyd CE, Massaut L (1999) Risks associated with the use of chemicals in pond aquaculture. Aquacult Eng 20:113–132. https://doi.org/10.1016/s0144-8609(99)00010-2

Boyd CE, Wood CW, Chaney PL, Queiroz JF (2010) Role of aquaculture pond sediments in sequestration of annual global carbon emissions. Environ Pollut 158:2537–2540. https://doi.org/10.1016/j.envpol.2010.04.025

Brooks ME, Kristensen K, Benthem KJ, van Magnusson A et al (2017) GLMMTMB balances speed and flexibility among packages for zero-inflated generalized linear mixed modeling. R Journal 9:378. https://doi.org/10.32614/rj-2017-066

Casper P, Maberly SC, Hall GH, Finlay BJ (2000) Fluxes of methane and carbon dioxide from a small productive lake to the atmosphere. Biogeochemistry 49:1–19. https://doi.org/10.1023/A:1006269900174

Castro HF, Williams NH, Ogram A (2000) Phylogeny of sulfate-reducing bacteria1. FEMS Microbiol Ecol 31:1–9. https://doi.org/10.1111/j.1574-6941.2000.tb00665.x

Czatzkowska M, Harnisz M, Korzeniewska E, Koniuszewska I (2020) Inhibitors of the methane fermentation process with particular emphasis on the microbiological aspect: a review. Energy Sci Eng 8:1880–1897. https://doi.org/10.1002/ese3.609

de Montety V, Martin JB, Cohen MJ, Foster C, Kurz MJ (2011) Influence of diel biogeochemical cycles on carbonate equilibrium in a Karst River. Chem Geol. https://doi.org/10.1016/j.chemgeo.2010.12.025

DelVecchia AG, Gougherty S, Taylor BW, Wissinger SA (2021) Biogeochemical characteristics and hydroperiod affect carbon dioxide flux rates from exposed high-elevation pond sediments. Limnol Oceanogr 66:1050–1067. https://doi.org/10.1002/lno.11663

Downing JA, Prairie YT, Cole JJ et al (2006) The global abundance and size distribution of lakes, ponds, and impoundments. Limnol Oceanogr 51:2388–2397. https://doi.org/10.4319/lo.2006.51.5.2388

Downing JA, Cole JJ, Middelburg JJ et al (2008) Sediment organic carbon burial in agriculturally eutrophic impoundments over the Last Century. Global Biogeochem Cy. https://doi.org/10.1029/2006gb002854

Elberling B, Askaer L, Jørgensen CJ, Joensen HP, Kühl M, Glud RN, Lauritsen FR (2011) Linking soil O_2, CO_2, and CH_4 concentrations in a wetland soil: implications for CO_2 and CH_4 fluxes. Environ Sci Technol 45:3393–3399. https://doi.org/10.1021/es103540k

Emilson EJ, Carson MA, Yakimovich KM et al (2018) Climate-driven shifts in sediment chemistry enhance methane production in Northern Lakes. Nat Commun. https://doi.org/10.1038/s41467-018-04236-2

Ertürk Arı P, Karakaya N, Evrendilek F (2021) Juxtaposing the spatiotemporal drivers of sediment CO_2, CH_4, and N_2O effluxes along ecoregional, wet-dry, and diurnal gradients. Atoms Pollut Res 12:160–171. https://doi.org/10.1016/j.apr.2021.03.002

Ettwig KF, Zhu B, Speth D, Keltjens JT, Jetten MS, Kartal B (2016) Archaea catalyze iron-dependent anaerobic oxidation of methane. P Natl Acad Sci 113:12792–12796. https://doi.org/10.1073/pnas.1609534113

Fairbairn L, Rezanezhad F, Gharasoo M, Parsons CT, Macrae ML, Slowinski S, Van Cappellen P (2023) Relationship between soil CO_2 fluxes and soil moisture: anaerobic sources explain fluxes at high water content. Geoderma 434:116493. https://doi.org/10.1016/j.geoderma.2023.116493

Fan L, Shahbaz M, Ge T, Wu J, Dippold M, Thiel V, Kuzyakov Y, Dorodnikov M (2019) To shake or not to shake: ^{13}C-based evidence on anaerobic methane oxidation in paddy soil. Soil Biol Biochem 133:146–154. https://doi.org/10.1016/j.soilbio.2019.03.010

Fan L, Dippold MA, Thiel V, Ge T, Wu J, Kuzyakov Y, Dorodnikov M (2021) Temperature sensitivity of anaerobic methane oxidation versus methanogenesis in paddy soil: implications for the CH_4 balance under global warming. Global Change Biol 28:654–664. https://doi.org/10.1111/gcb.15935

Fromin N, Pinay G, Montuelle B, Landais D, Ourcival JM, Joffre R, Lensi R (2010) Impact of seasonal sediment desiccation and rewetting on microbial processes involved in greenhouse gas emissions. Ecohydrology 3:339–348. https://doi.org/10.1002/eco.115

Gauthier M, Bradley RL, Šimek M (2015) More evidence that anaerobic oxidation of methane is prevalent in soils: is it time to upgrade our biogeochemical models. Soil Biol Biochem 80:167–174. https://doi.org/10.1016/j.soilbio.2014.10.009

Gilbert PJ, Cooke DA, Deary M, Taylor S, Jeffries MJ (2017) Quantifying rapid spatial and temporal variations of CO_2 fluxes from small, lowland freshwater ponds. Hydrobiologia 793:83–93. https://doi.org/10.1007/s10750-016-2855-y

Gómez-Gener L, Obrador B, von Schiller D et al (2015) Hot spots for carbon emissions from Mediterranean fluvial networks during summer drought. Biogeochemistry 125:409–426. https://doi.org/10.1007/s10533-015-0139-7

Gupta V, Smemo KA, Yavitt JB, Fowle D, Branfireun B, Basiliko N (2013) Stable isotopes reveal widespread anaerobic methane oxidation across latitude and peatland type. Environ Sci Technol 47:8273–8279. https://doi.org/10.1021/es400484t

Hamer U, Makeschin F, Stadler J, Klotz S (2008) Soil organic matter and microbial community structure in set-aside and intensively managed arable soils in NE-Saxony, Germany. Appl Soil Ecol 40:465–475. https://doi.org/10.1016/j.apsoil.2008.07.001

Haque MM, Biswas JC, Kim SY, Kim PJ (2015) Suppressing methane emission and global warming potential from rice fields through intermittent drainage and Green Biomass Amendment. Soil Use Manage 32:72–79. https://doi.org/10.1111/sum.12229

Haroon MF, Hu S, Shi Y, Imelfort M, Keller J, Hugenholtz P, Yuan Z, Tyson GW (2013) Anaerobic oxidation of methane coupled to nitrate reduction in a novel archaeal lineage. Nature 500:567–570. https://doi.org/10.1038/nature12375

Hartig F (2022) DHARMa: Residual Diagnostics for Hierarchical (Multi-Level Mixed) Regression Models. R package version 0.4.6, https://CRAN.R-project.org/package=DHARMa

Hatala JA, Detto M, Sonnentag O, Deverel SJ, Verfaillie J, Baldocchi DD (2012) Greenhouse gas (CO_2, CH_4, H_2O) fluxes from drained and flooded agricultural peatlands in the Sacramento-San Joaquin delta. Agr Ecosyst Environ 150:1–18. https://doi.org/10.1016/j.agee.2012.01.009

Holgerson MA (2015) Drivers of carbon dioxide and methane supersaturation in small, temporary ponds. Biogeochemistry 124:305–318. https://doi.org/10.1007/s10533-015-0099-y

Holgerson MA, Raymond PA (2016) Large contribution to inland water CO_2 and CH_4 emissions from very small ponds. Nat Geosci 9:222–228. https://doi.org/10.1038/NGEO2654

Hu Z, Gu C, Maucieri C, Shi F, Zhao Y, Feng C, Cao Y, Zhang Y (2022) Crayfish–fish aquaculture ponds exert reduced climatic impacts and higher economic benefits than traditional wheat–rice paddy cultivation. Agriculture 12:515. https://doi.org/10.3390/agriculture12040515

Huffman FG (2003) Uronic acids.In: Encyclopedia of Food Sciences and Nutrition. Elsevier: Amsterdam, pp 5890–5896. https://doi.org/10.1016/b0-12-227055-x/01221-9

IPCC (2021) Climate Change 2021: The Physical Science Basis. Contribution of Working Group I to the Sixth Assessment Report of the Intergovernmental Panel on Climate Change Masson-Delmotte V, Zhai P, Pirani A et al. Cambridge University Press, Cambridge, United Kingdom and New York, NY, USA, p 2391. https://doi.org/10.1017/9781009157896

Jacquemin J, Costa Gomes MF, Husson P, Majer V (2006) Solubility of carbon dioxide, ethane, methane, oxygen, nitrogen, hydrogen, argon, and carbon monoxide in 1-butyl-3-methylimidazolium tetrafluoroborate between temperatures 283k and 343K and at pressures close to atmospheric. J Chem Thermodyn 38:490–502. https://doi.org/10.1016/j.jct.2005.07.002

Jin H, Yoon TK, Lee SH, Kang H, Im J, Park JH (2016) Enhanced greenhouse gas emission from exposed sediments along a hydroelectric reservoir during an extreme drought event. Environ Res Lett 11:124003. https://doi.org/10.1088/1748-9326/11/12/124003

Joergensen RG (1996) The fumigation-extraction method to estimate soil microbial biomass: calibration of the K_{ec} value. Soil Biol Biochem 28:25–31. https://doi.org/10.1016/0038-0717(95)00102-6

Kassambara A, Mundt F (2020) factoextra: Extract and Visualize the Results of Multivariate Data Analyses_R package version 1.0.7, https://CRAN.R-project.org/package=factoextra

Keiluweit M, Wanzek T, Kleber M, Nico P, Fendorf S (2017) Anaerobic microsites have an unaccounted role in soil carbon stabilization. Nat Commun. https://doi.org/10.1038/s41467-017-01406-6

Keller PS, Catalán N, von Schiller D et al (2020) Global CO2 emissions from dry inland waters share common drivers across ecosystems. Nat Commun. https://doi.org/10.1038/s41467-020-15929-y

Kim J, Chaudhary DR, Lee J et al (2020) Microbial mechanism for enhanced methane emission in deep soil layer of phragmites-introduced Tidal Marsh. Environ Int 134:105251. https://doi.org/10.1016/j.envint.2019.105251

Knorr KH, Glaser B, Blodau C (2008) Fluxes and ^{13}C isotopic composition of dissolved carbon and pathways of methanogenesis in a fen soil exposed to experimental drought. Biogeosciences 5:1457–1473. https://doi.org/10.5194/bg-5-1457-2008

Kokou F, Fountoulaki E (2018) Aquaculture waste production associated with antinutrient presence in common fish feed plant ingredients. Aquaculture 495:295–310. https://doi.org/10.1016/j.aquaculture.2018.06.003

Kosten S, Roland F, Da Motta Marques DM et al (2010) Climate-dependent CO2 emissions from lakes. Global Biogeochem Cy. https://doi.org/10.1029/2009gb003618

Kramer MG, Lajtha K, Aufdenkampe AK (2017) Depth trends of soil organic matter C: N and 15N natural abundance controlled by association with minerals. Biogeochemistry 136:237–248. https://doi.org/10.1007/s10533-017-0378-x

Kumaraswamy S, Ramakrishnan B, Sethunathan N (2001) Methane production and oxidation in an anoxic rice soil as influenced by inorganic redox species. J Environ Qual 30:2195–2201. https://doi.org/10.2134/jeq2001.2195

Lê S, Josse J, Husson F (2008) factominer: anrpackage for multivariate analysis. J Stat Softw. https://doi.org/10.18637/jss.v025.i01

Le Mer J, Roger P (2001) Production, oxidation, emission and consumption of methane by soils: a review. Eur J Soil Biol 37:25–50. https://doi.org/10.1016/s1164-5563(01)01067-6

Lenth R (2024) emmeans: Estimated Marginal Means, aka Least-Squares Means. R package version 1.10.1, https://CRAN.R-project.org/package=emmeans

Lüdecke D (2023) sjPlot: Data Visualization for Statistics in Social Science. R package version 2.8.14. https://CRAN.R-project.org/package=sjPlot

Ma Y, Sun L, Liu C et al (2018) A comparison of methane and nitrous oxide emissions from inland mixed-fish and crab aquaculture ponds. Sci Total Environ 637–638:517–523. https://doi.org/10.1016/j.scitotenv.2018.05.040

Marcé R, Obrador B, Gómez-Gener L et al (2019) Emissions from dry inland waters are a blind spot in the global carbon cycle. Earth Sci Rev 188:240–248. https://doi.org/10.1016/j.earscirev.2018.11.012

Martinsen KT, Kragh T, Sand-Jensen K (2019) Carbon dioxide fluxes of air-exposed sediments and desiccating ponds. Biogeochemistry 144:165–180. https://doi.org/10.1007/s10533-019-00579-0

Mathijssen PJH, Gałka M, Borken W, Knorr KH (2019) Plant communities control long term carbon accumulation and biogeochemical gradients in a Patagonian bog. Sci Total Environ 684:670–681. https://doi.org/10.1016/j.scitotenv.2019.05.310

Mohanty SR, Kollah B, Sharma VK, Singh AB, Singh M, Rao AS (2013) Methane oxidation and methane driven redox process during sequential reduction of a flooded soil ecosystem. Ann Microbiol 64:65–74. https://doi.org/10.1007/s13213-013-0633-x

Mohanty SR, Bandeppa GS, Dubey G, Ahirwar U, Patra AK, Bharati K (2017) Methane oxidation in response to iron reduction-oxidation metabolism in tropical soils. Eur J Soil Biol 78:75–81. https://doi.org/10.1016/j.ejsobi.2016.08.007

Muyzer G, Stams AJ (2008) The ecology and biotechnology of sulphate-reducing bacteria. Nat Rev Microbiol 6:441–454. https://doi.org/10.1038/nrmicro1892

Pandey A, Mai VT, Vu DQ, Bui TP, Mai TL, Jensen LS, de Neergaard A (2014) Organic matter and water management strategies to reduce methane and nitrous oxide emissions from rice paddies in Vietnam. Agr Ecosyst Environ 196:137–146. https://doi.org/10.1016/j.agee.2014.06.010

Paranaíba JR, Aben R, Barrosa N et al (2022) Cross-continental importance of CH_4 emissions from dry inland-waters. Sci Tot Env 814:151925. https://doi.org/10.1016/j.scitotenv.2021.151925

Parkin TB, Doran JW, Franco-Vizcaino E (1997) Field and laboratory tests of soil respiration. SSSA Special Public. https://doi.org/10.2136/sssaspecpub49.c14

Pinto R, Weigelhofer G, Brito AG, Hein T (2021) Effects of dry-wet cycles on nitrous oxide emissions in freshwater sediments: a synthesis. PeerJ. https://doi.org/10.7717/peerj.10767

Praetzel LS, Plenter N, Schilling S, Schmiedeskamp M, Broll G, Knorr KH (2020) Organic matter and sediment properties determine in-lake variability of sediment CO_2 and CH_4 production and emissions of a small and Shallow Lake. Biogeosciences 17:5057–5078. https://doi.org/10.5194/bg-17-5057-2020

R Core Team (2023) R: A language and environment for statistical computing. R Foundation for Statistical Computing, Vienna, Austria. https://www.R-project.org/

Raymond PA, Hartmann J, Lauerwald R et al (2013) Global carbon dioxide emissions from Inland Waters. Nature 503:355–359. https://doi.org/10.1038/nature12760

Richardson DC, Holgerson MA, Farragher MJ et al (2022) A functional definition to distinguish ponds from lakes and wetlands. Sci Rep 12:10472. https://doi.org/10.1038/s41598-022-14569-0

Rogers DB, Newcomer ME, Raberg JH et al (2021) Modeling the impact of riparian hollows on river corridor nitrogen exports. Front Water. https://doi.org/10.3389/frwa.2021.590314

Rosentreter JA, Borges AV, Deemer BR et al (2021) Half of global methane emissions come from highly variable aquatic ecosystem sources. Nat Geosci 14:225–230. https://doi.org/10.1038/s41561-021-00715-2

Sander R (2015) Compilation of Henry's law constants (version 4.0) for water as solvent. Atmos Chem Phys 15:4399–4981. https://doi.org/10.5194/acp-15-4399-2015

Schimel JP (2018) Life in dry soils: effects of drought on soil microbial communities and processes. Annu Rev Ecol Evol Syst 49:409–432. https://doi.org/10.1146/annurev-ecolsys-110617-062614

Schmiedeskamp M, Praetzel LS, Bastviken D, Knorr KH (2021) Whole-lake methane emissions from two temperate shallow lakes with fluctuating water levels: relevance of spatiotemporal patterns. Limnol Oceanogr 66:2455–2469. https://doi.org/10.1002/lno.11764

Shen L, Tian M, Cheng H, Liu X, Yang Y, Liu J, Xu J, Kong Y, Li J, Liu Y (2020) Different responses of nitrite and nitrate-dependent anaerobic methanotrophs to increasing nitrogen loading in a freshwater reservoir. Environ Pollut 263:114623. https://doi.org/10.1016/j.envpol.2020.114623

Smemo KA, Yavitt JB (2007) Evidence for anaerobic CH_4 oxidation in freshwater peatlands. Geomicrobiol J 24:583–597. https://doi.org/10.1080/01490450701672083

Smemo KA, Yavitt JB (2011) Anaerobic oxidation of methane: an underappreciated aspect of methane cycling in peatland ecosystems? Biogeosciences 8:779–793. https://doi.org/10.5194/bg-8-779-2011

Sobek S, Durisch-Kaiser E, Zurbrügg R, Wongfun N, Wessels M, Pasche N, Wehrli B (2009) Organic carbon burial efficiency in lake sediments controlled by oxygen exposure time and sediment source. Limnol Oceanogr 54:2243–2254. https://doi.org/10.4319/lo.2009.54.6.2243

Stadmark J, Leonardson L (2007) Greenhouse gas production in a pond sediment: effects of temperature, nitrate, acetate and season. Sci Total Environ 387:194–205. https://doi.org/10.1016/j.scitotenv.2007.07.039

Stumm W, Morgan JJ (1995) Aquatic chemistry: chemical equilibria and rates in natural waters, 3rd edn. Wiley, New York

Szal D, Gruca-Rokosz R (2020) Anaerobic oxidation of methane in freshwater sediments of Rzeszów Reservoir. Water 12:398. https://doi.org/10.3390/w12020398

Teatini P, Tosi L, Strozzi T (2011) Quantitative evidence that compaction of Holocene sediments drives the present land subsidence of the Po Delta, Italy. J Geophys Res. https://doi.org/10.1029/2010jb008122

Tranvik LJ, Downing JA, Cotner JB et al (2009) Lakes and reservoirs as regulators of carbon cycling and climate. Limnol Oceanogr 54:2298–2314. https://doi.org/10.4319/lo.2009.54.6_part_2.2298

Tuyishime O, Strömgren M, Joel A, Messing I, Naramabuye FX, Wesström I (2022) Deep drainage lowers methane and nitrous oxide emissions from rice fields in a semi-arid environment in Rwanda. Soil Syst 6:84. https://doi.org/10.3390/soilsystems6040084

Valentine DL (2002) Biogeochemistry and microbial ecology of methane oxidation in anoxic environments: a review. Antonie Van Leewenhoek 81:271–282. https://doi.org/10.1023/a:1020587206351

van Bergen TJ, Barros N, Mendonça R et al (2019) Seasonal and diel variation in greenhouse gas emissions from an urban pond and its major drivers. Limnol Oceanogr 64:2129–2139. https://doi.org/10.1002/lno.11173

Vigderovich H, Eckert W, Elul M, Rubin-Blum M, Elvert M, Sivan O (2022) Long-term incubations provide insight into the mechanisms of anaerobic oxidation of methane in methanogenic lake sediments. Biogeosciences 19:2313–2331. https://doi.org/10.5194/bg-19-2313-2022

Wang G, Xia X, Liu S, Zhang S, Yan W, McDowell WH (2021) Distinctive patterns and controls of nitrous oxide concentrations and fluxes from urban inland waters. Environ Sci Technol 55:8422–8431. https://doi.org/10.1021/acs.est.1c00647

Wickham H (2016) ggplot2: elegant graphics for data analysis. Springer-Verlag, New York

Woszczyk M, Bechtel A, Ceslinski R (2011) Interactions between microbial degradation of sedimentary organic matter and lake hydrodynamics in shallow water bodies: Insights from Lake Sarbsko (Northern Poland). J Limnol 70:293. https://doi.org/10.4081/jlimnol.2011.293

Wrage N, Velthof GL, van Beusichem ML, Oenema O (2001) Role of nitrifier denitrification in the production of nitrous oxide. Soil Biol Biochem 33:1723–1732. https://doi.org/10.1016/s0038-0717(01)00096-7

Wu J, Joergensen RG, Pommerening B, Chaussod R, Brookes PC (1990) Measurement of soil microbial biomass C by fumigation-extraction-an automated procedure. Soil Biol Biochem 22:1167–1169. https://doi.org/10.1016/0038-0717(90)90046-3

Yang J, Liu J, Hu X, Li X, Wang Y, Li H (2013) Effect of water table level on CO_2, CH_4 and N_2O emissions in a freshwater marsh of Northeast China. Soil Biol Biochem 61:52–60. https://doi.org/10.1016/j.soilbio.2013.02.009

Yang P, He Q, Huang J, Tong C (2015) Fluxes of greenhouse gases at two different aquaculture ponds in the coastal zone of Southeastern China. Atoms Environ 115:269–277. https://doi.org/10.1016/j.atmosenv.2015.05.067

Yu K, Xiao S, Zheng F, Fang X, Zou J, Liu S (2023) A greater source of methane from drainage rivers than from rice paddies with drainage practices in Southeast China. Agr Ecosyst Environ 345:108321. https://doi.org/10.1016/j.agee.2022.108321

Yuan J, Xiang J, Liu D, Kang H, He T, Kim S, Lin Y, Freeman C, Ding W (2019) Rapid growth in greenhouse gas emissions from the adoption of industrial-scale aquaculture. Nat Clim Change 9:318–322. https://doi.org/10.1038/s41558-019-0425-9

Zeng FW, Masiello CA, Hockaday WC (2011) Controls on the origin and cycling of riverine dissolved inorganic carbon in the Brazos River, Texas. Biogeochemistry 104:275–291. https://doi.org/10.1007/s10533-010-9501-y

Zhao M, Han G, Li J, Song W, Qu W, Elle F, Wang J, Jiang C (2020) Responses of soil CO_2 and CH_4 emissions to changing water table level in a coastal wetland. J Clean Prod 269:122316. https://doi.org/10.1016/j.jclepro.2020.122316

Zheng J, Thornton PE, Painter SL, Gu B, Wullschleger SD, Graham DE (2019) Modeling anaerobic soil organic carbon decomposition in Arctic polygon tundra: Insights into soil geochemical influences on carbon mineralization. Biogeosciences 16:663–680. https://doi.org/10.5194/bg-16-663-2019